Water Resources Research

RESEARCH ARTICLE
10.1029/2019WR026058

ECOSTRESS: NASA's Next Generation Mission to Measure Evapotranspiration From the International Space Station

Joshua B. Fisher[1], Brian Lee[1], Adam J. Purdy[1], Gregory H. Halverson[1], Matthew B. Dohlen[1], Kerry Cawse-Nicholson[1], Audrey Wang[1], Ray G. Anderson[2], Bruno Aragon[3], M. Altaf Arain[4], Dennis D. Baldocchi[5], John M. Baker[6], Hélène Barral[7], Carl J. Bernacchi[8,9], Christian Bernhofer[10], Sébastien C. Biraud[11], Gil Bohrer[12], Nathaniel Brunsell[13], Bernard Cappelaere[7], Saulo Castro-Contreras[14], Junghwa Chun[15], Bryan J. Conrad[13], Edoardo Cremonese[16], Jérôme Demarty[7], Ankur R. Desai[17], Anne De Ligne[18], Lenka Foltýnová[19], Michael L. Goulden[20], Timothy J. Griffis[21], Thomas Grünwald[10], Mark S. Johnson[22], Minseok Kang[23], Dave Kelbe[24], Natalia Kowalska[19], Jong-Hwan Lim[15], Ibrahim Maïnassara[7,25], Matthew F. McCabe[3], Justine E.C. Missik[26], Binayak P. Mohanty[27], Caitlin E. Moore[8], Laura Morillas[22], Ross Morrison[28], J. William Munger[29], Gabriela Posse[30], Andrew D. Richardson[31,32], Eric S. Russell[33], Youngryel Ryu[34], Arturo Sanchez-Azofeifa[14], Marius Schmidt[35], Efrat Schwartz[36], Iain Sharp[14], Ladislav Šigut[19], Yao Tang[37], Glynn Hulley[1], Martha Anderson[38], Christopher Hain[39], Andrew French[40], Eric Wood[41], and Simon Hook[1]

[1]Jet Propulsion Laboratory, California Institute of Technology, Pasadena, CA, USA, [2]U.S. Department of Agriculture, Riverside, CA, USA, [3]Hydrology, Agriculture and Land Observation Group (HALO), Division of Biological and Environmental Science and Engineering, King Abdullah University of Science and Technology, Thuwal, Saudi Arabia, [4]School of Geography and Earth Sciences, McMaster University, Hamilton, Ontario, Canada, [5]Department of Environmental Science, Policy and Management, University of California, Berkeley, CA, USA, [6]U.S. Department of Agriculture, St. Paul, MN, USA, [7]HydroSciences Montpellier (HSM), University Montpellier, CNRS, IRD, Montpellier, France, [8]Center for Advanced Bioenergy and Bioproducts Innovation, Institute for Sustainability, Energy, and Environment and Carl R. Woese Institute for Genomic Biology, University of Illinois Urbana-Champaign, Urbana, IL, USA, [9]U.S. Department of Agriculture, Global Change and Photosynthesis Research Unit, Urbana, IL, USA, [10]Technische Universität Dresden, Institute of Hydrology and Meteorology, Tharandt, Germany, [11]Lawrence Berkeley National Laboratory, Berkeley, CA, USA, [12]Department of Civil, Environmental and Geodetic Engineering, Ohio State University, Columbus, OH, USA, [13]Department of Geography and Atmospheric Science, University of Kansas, Lawrence, KS, USA, [14]Centre for Earth Observation Sciences (CEOS), Earth and Atmospheric Sciences Department, University of Alberta, Edmonton, Alberta, Canada, [15]National Institute of Forest Science, Seoul, South Korea, [16]Environmental Protection Agency of Aosta Valley, Aosta, Italy, [17]Department of Atmospheric and Oceanic Sciences, University of Wisconsin-Madison, Madison, WI, USA, [18]TERRA Teaching and Research Centre, Gembloux Agro-Bio Tech, University of Liege, Gembloux, Belgium, [19]Global Change Research Institute, Czech Academy of Sciences, Brno, Czech Republic, [20]Department of Earth System Science, University of California, Irvine, CA, USA, [21]Department of Soil, Water, and Climate, University of Minnesota, Twin Cities, St. Paul, MN, USA, [22]Department of Earth, Ocean, and Atmospheric Sciences, University of British Columbia, Vancouver, British Columbia, Canada, [23]National Center for AgroMeteorology, Seoul, South Korea, [24]Xerra Earth Observation Institute, Alexandra, New Zealand, [25]Représentation de l'IRD au Niger, Niamey, Niger, [26]Laboratory for Atmospheric Research, Department of Civil and Environmental Engineering, Washington State University, Pullman, WA, USA, [27]Texas Water Observatory, Texas A&M University, College Station, TX, USA, [28]Centre for Ecology and Hydrology, Wallingford, UK, [29]School of Engineering and Applied Sciences, Harvard University, Cambridge, MA, USA, [30]Instituto de Clima y Agua. INTA, Buenos Aires, Argentina, [31]Center for Ecosystem Science and Society, Northern Arizona University, Flagstaff, AZ, USA, [32]School of Informatics, Computing, and Cyber Systems, Northern Arizona University, Flagstaff, AZ, USA, [33]Department of Civil and Environmental Engineering, Washington State University, Pullman, WA, USA, [34]Department of Landscape Architecture and Rural Systems Engineering, Seoul National University, Seoul, South Korea, [35]Institute of Bio- and Geosciences: Agrosphere (IBG-3) Forschungszentrum Jülich IBG-3, Jülich, Germany, [36]Department of Earth and Planetary Sciences, Weizmann Institute of Science, Rehovot, Israel, [37]School of Civil and Environmental Engineering, Georgia Institute of Technology, Atlanta, GA, USA, [38]U.S. Department of Agriculture-Agricultural Research Service, Beltsville, MD, USA, [39]NASA Marshall Space Flight Center, Huntsville, AL, USA, [40]U.S. Department of Agriculture, Maricopa, AZ, USA, [41]Department of Civil and Environmental Engineering, Princeton University, Princeton, NJ, USA

Key Points:
- ECOSTRESS is a state-of-the-art combination of thermal bands, spatial and temporal resolutions, and measurement accuracy and precision
- Data from 82 eddy covariance sites were coalesced concurrently with the first year of ECOSTRESS for Stage 1 validation
- Clear-sky ET from ECOSTRESS compared well against a wide range of eddy covariance sites, vegetation classes, climate zones, and times of day

Supporting Information:
- Supporting Information S1

Correspondence to:
J. B. Fisher,
joshbfisher@gmail.com

Citation:
Fisher, J. B., Lee, B., Purdy, A. J., Halverson, G. H., Dohlen, M. B., Cawse-Nicholson, K., et al. (2020). ECOSTRESS: NASA's Next Generation Mission to measure evapotranspiration from the International Space Station. *Water Resources Research*, *56*, e2019WR026058. https://doi.org/10.1029/2019WR026058

Received 29 JUL 2019
Accepted 25 MAR 2020
Accepted article online 6 APR 2020

Abstract The ECOsystem Spaceborne Thermal Radiometer Experiment on Space Station (ECOSTRESS) was launched to the International Space Station on 29 June 2018 by the National Aeronautics and Space Administration (NASA). The primary science focus of ECOSTRESS is centered on evapotranspiration (ET), which is produced as Level-3 (L3) latent heat flux (*LE*) data products. These data are generated from the Level-2 land surface temperature and emissivity product (L2_LSTE), in conjunction with ancillary surface and atmospheric data. Here, we provide the first validation (Stage 1, preliminary) of the global ECOSTRESS clear-sky ET product (L3_ET_PT-JPL, Version 6.0) against *LE* measurements at 82 eddy covariance sites around the world. Overall, the ECOSTRESS ET product performs well against the site measurements (clear-sky instantaneous/time of overpass: $r^2 = 0.88$; overall bias = 8%; normalized root-mean-square error, RMSE = 6%). ET uncertainty was generally consistent across climate zones, biome types, and times of day (ECOSTRESS samples the diurnal cycle), though temperate sites are overrepresented. The 70-m-high spatial resolution of ECOSTRESS improved correlations by 85%, and RMSE by 62%, relative to 1-km pixels. This paper serves as a reference for the ECOSTRESS L3 ET accuracy and Stage 1 validation status for subsequent science that follows using these data.

1. Introduction

Remote sensing of evapotranspiration (ET) has advanced substantially over the past few decades (Fisher et al., 2017). ET data are produced from a wide range of airborne and spaceborne sensors, instruments, and missions from high spatial resolution to global coverage (Allen et al., 2007; Anderson et al., 2011; Fisher et al., 2008; Miralles et al., 2011; Mu et al., 2011; Su, 2002). These data are used in, for example, biodiversity assessments (Fisher et al., 2011; Gaston, 2000), regional water balance closures (Armanios & Fisher, 2014; Y. Chen et al., 2014; Marshall et al., 2012; Sahoo et al., 2011), studies of climate and cloud formation (Mölders & Raabe, 1996; Rabin et al., 1990; Shukla & Mintz, 1982), agricultural management (Allen et al., 1998; Allen et al., 2011; Farahani et al., 2007), water resources decision-making (Anderson et al., 2012; Bastiaanssen et al., 2005), detection of drought and heat waves (Miralles et al., 2014; Otkin et al., 2014; Rind et al., 1990; Vicente-Serrano et al., 2010), urban heat islands (Oke, 1982; Taha, 1997), and water rights litigation (Allen et al., 2005; Anderson et al., 2012). Nonetheless, until recently, there remained a large gap in our ability to monitor ET concurrently at both fine spatial and fine temporal scales globally. For example, Landsat has provided fine spatial resolution (>60 m) but poor temporal resolution (16 days); Moderate resolution Imaging Spectroradiometer (MODIS)/Visible Infrared Imaging Radiometer Suite has provided fine temporal resolution (daily), but moderate spatial resolution (≥375 m) (Allen et al., 2011, 2007; Anderson et al., 2012; X. Chen et al., 2008; Kilic et al., 2016). As polar orbiters, all of these missions miss the diurnal cycle, passing over the same spot on Earth at the same time, every time. On the other hand, geostationary satellites such as GOES capture the diurnal cycle, but lack cohesive global coverage, and suffer from even worse spatial resolution (>3 km) (Fisher et al., 2017).

The ECOsystem Spaceborne Thermal Radiometer Experiment on Space Station (ECOSTRESS) was launched to the International Space Station (ISS) on 29 June 2018. ECOSTRESS is a thermal radiometer built by National Aeronautics and Space Administration (NASA)'s Jet Propulsion Laboratory (JPL) that measures thermal infrared radiation (TIR) in five bands from 8- to 12.5-μm wavelengths, plus an additional sixth band at 1.6 μm for geolocation and cloud detection (ecostress.jpl.nasa.gov). On board the ISS, which has an irregular orbit (rather than a regular polar or geostationary orbit), ECOSTRESS collects measurements continuously between ~52°N and ~52°S at different times of day. The overpass return frequency for any same spot on Earth is 1–5 days, depending on latitude, with some areas measured multiple times in a single day (particularly the higher latitudes where the ISS orbital direction shifts) within the ECOSTRESS swath width of 384 km (Figure 1). The pixel size at nadir is 38 m × 69 m, which is resampled by the ECOSTRESS data production software to 70-m × 70-m pixels for noise reduction and ease of use. As such, ECOSTRESS now provides a combination of good spatial and temporal resolutions with diurnal cycle sampling.

ECOSTRESS produces four levels of data products, with each increasing level incorporating additional ancillary information. The first data-product level includes raw instrument and calibration information (L0-1A) (Logan & Johnson, 2015), calibrated at-sensor radiances (L1B_RAD), and geolocation (L1B_GEO) (Smyth & Leprince, 2018). The second data-product level incorporates additional data from numerical weather

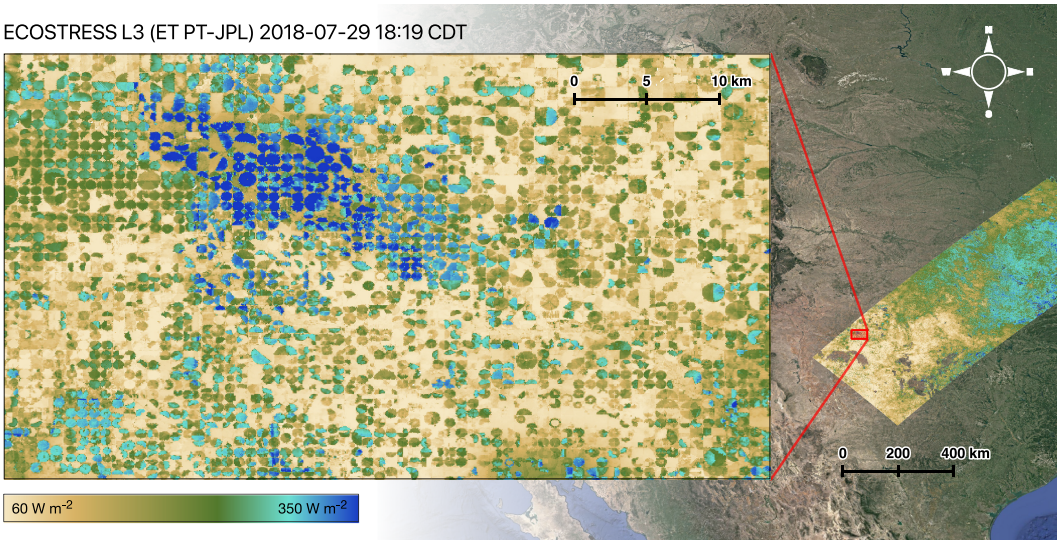

Figure 1. The 384-km swath width, high spatial resolution (70 m × 70 m) and accuracy of ECOSTRESS provide field-scale detail and large coverage of evapotranspiration worldwide. Here, ECOSTRESS is acquiring data over Texas, USA, showing differences between pivot irrigation fields as well as within fields.

prediction for atmospheric correction (Malakar & Hulley, 2016; Matricardi, 2008; Saunders et al., 1999) to generate land surface temperature and emissivity (L2_LSTE) and a cloud mask (L2_CLOUD) using the Temperature and Emissivity Separation retrieval algorithm also used in other missions (Gillespie et al., 1998; Hulley et al., 2017; Hulley & Hook, 2011; Hulley & Hook, 2018). The third data-product level incorporates additional atmospheric data from MODIS and surface properties from MODIS and Landsat to generate ET (as the latent heat flux, *LE*), including the ET components of canopy transpiration, soil evaporation, and interception evaporation using the Priestley-Taylor (PT) JPL retrieval algorithm (L3_ET_PT-JPL) (Fisher et al., 2008; Fisher & ECOSTRESS algorithm development team, 2015; Halverson, 2018). An additional ET product (L3_ET_ALEXI) is produced for a subset of agricultural sites in the United States with the Disaggregated Atmosphere-Land Exchange Inverse model (Anderson, Kustas, et al., 2013). Finally, the fourth data product level includes a stress index based on the Evaporative Stress Index (ESI) (Anderson et al., 2010; Anderson, Hain, et al., 2013; Otkin et al., 2013) (L4_ESI_PT-JPL; L4_ESI_ALEXI), and a water use efficiency (WUE) product (L4_WUE) (Fisher & ECOSTRESS algorithm development team, 2018), the latter of which originally incorporated gross primary production from MODIS (Zhao et al., 2005), but switched to a native 70 m gross primary production product retrieved using the Breathing Earth System Simulator algorithm (Ryu et al., 2011).

At the outset, the ECOSTRESS Early Adopters program was the largest in NASA history, with a large community of scientists using ECOSTRESS data for a wide variety of applications (ecostress.jpl.nasa.gov/early--adopters). NASA develops Early Adopters programs for new missions to enable support for learning to use the data products while the mission and data production are still in development. Nonetheless, it is essential that ECOSTRESS data are validated first to provide an assessment of accuracy and error before these scientific investigations can be established. Validation is a necessary and important first step to launch these science investigations forward. First, the L1 and L2 products were validated in Hook et al. (2019), who reported uncertainties for those products at <1 K. The objective of this study is to conduct the initial validation and error assessment of the global ECOSTRESS ET product (L3_ET_PT-JPL). Specifically, we ask: how well does ECOSTRESS capture ET across different biome types and climate zones? Are there biases in ECOSTRESS across different times of day?

To conduct this analysis, we used ET measurements from eddy covariance sites (Baldocchi, 2008; Baldocchi et al., 2001). Typically, eddy covariance data sets require many months to years for systematic collection, organization, consistency, gap-filling, energy balance closure, spike removal, quality flags, and other processing procedures (Baldocchi, 2003; Falge et al., 2001; Foken, 2008; Moffat et al., 2007; Papale et al., 2006; Wilson et al., 2002). In order to develop an initial preliminary and fast error assessment for ECOSTRESS

to allow the science community to proceed forward, we collected as large a data set as fast as possible, conducting a rapid processing of data from over a hundred disparate eddy flux sites. Consequently, we classify this as the Land Product Validation Stage 1 (Committee on Earth Observation Satellites; lpvs.gsfc.nasa.gov), or preliminary validation, with the understanding that both future refined eddy flux-based validation data sets and fully processed versions will become available, as well as further reprocessing for future versions of the ECOSTRESS data.

2. Methods

2.1. ECOSTRESS ET Data

The ET retrieval approach for the ECOSTRESS L3_ET_PT-JPL product is the PT-JPL algorithm (Fisher et al., 2008), which has been widely validated throughout the literature as one of the top performing global remote sensing ET models (e.g., Y. Chen et al., 2014; Ershadi et al., 2014; Gomis-Cebolla et al., 2019; Jiménez et al., 2018; McCabe et al., 2016; Michel et al., 2016; Miralles et al., 2016; Polhamus et al., 2013; Purdy et al., 2018; Talsma et al., 2018; Vinukollu et al., 2011). Through ecophysiological constraint functions, PT-JPL retrieves actual ET by reducing potential ET (PET) starting with the PT equation (Fisher et al., 2011; Priestley & Taylor, 1972):

$$PET = \alpha \frac{\Delta}{\Delta + \gamma} R_n \tag{1}$$

where Δ is the slope of the saturation-to-vapor pressure curve, dependent on near-surface air temperature (T_a; °C) and water vapor pressure (e_a; kPa), γ is the psychrometric constant (0.066 kPa/°C), R_n is net radiation (W/m^2), and α is the PT coefficient of 1.26 (unitless); PET is in units of W/m^2.

A series of ecophysiological scalar functions (unitless; 0–1), based on atmospheric vapor pressure deficit (D_a; kPa), relative humidity (RH; fraction), and vegetation indices, including normalized difference and soil adjusted vegetation indices (NDVI and SAVI; unitless), simultaneously reduce PET to actual ET, and partition total ET into three sources for canopy transpiration (ET_c), soil evaporation (ET_s), and interception evaporation (ET_i):

$$ET = ET_c + ET_s + ET_i \tag{2}$$

$$ET_c = (1 - f_{wet}) f_g f_T f_M \alpha \frac{\Delta}{\Delta + \gamma} R_{nc} \tag{3}$$

$$ET_s = (f_{wet} + f_{SM}(1 - f_{wet})) \alpha \frac{\Delta}{\Delta + \gamma} (R_{ns} - G) \tag{4}$$

$$ET_i = f_{wet} \alpha \frac{\Delta}{\Delta + \gamma} R_{nc} \tag{5}$$

$$f_T = e^{-\left(\frac{Ta - T_{opt}}{T_{opt}}\right)^2} \tag{6}$$

$$T_{opt} = T_{max}\ at\ max\left(R_n T_a \frac{SAVI}{D_a}\right) \tag{7}$$

where f_{wet} is relative surface wetness (RH^4) (Stone et al., 1977), f_g is green canopy fraction (f_{APAR}/f_{IPAR}) (Zhang et al., 2005), f_T is a plant temperature constraint (June et al., 2004; Potter et al., 1993), f_M is a plant moisture constraint ($f_{APAR}/f_{APARmax}$) (Potter et al., 1993), and f_{SM} is a soil moisture constraint (RH^{D_a}) (Bouchet, 1963; Fisher et al., 2008). f_{APAR} is absorbed photosynthetically active radiation (PAR), f_{IPAR} is intercepted PAR, T_{opt} (°C) is the optimum temperature linked to plant phenology, and G is the soil heat flux (W/m^2) (Purdy et al., 2016). R_{nc} and R_{ns} are R_n for the canopy and the soil, respectively, based on leaf area index derived from NDVI. PT-JPL is run globally and continuously in space and time with no need for calibration or site-specific parameters.

R_n is partitioned into the upward and downward shortwave and longwave components:

$$Rn = (R_{SD} - R_{SU}) + (R_{LD} - R_{LU}) \tag{8}$$

where R_{SD} is downwelling shortwave radiation, R_{SU} is upwelling shortwave radiation, R_{LD} is downwelling longwave radiation, and R_{LU} is upwelling longwave radiation. The R_n components are retrieved implementing the Forest Light Environmental Simulator (Iwabuchi, 2006; Kobayashi & Iwabuchi, 2008) and Breathing Earth System Simulator (Ryu et al., 2011, 2012, 2018). R_{SD} is calculated from eight inputs: (1) solar zenith angle, (2) aerosol optical thickness at 550 nm, (3) cloud optical thickness, (4) land surface albedo, (5) cloud top height, (6) atmospheric profile type, (7) aerosol type, and (8) cloud type (Ryu et al., 2018). R_{SU} is calculated from broadband surface albedo, which integrates black and white sky albedo, and R_{SD}. R_{LD} and R_{LU} are calculated from Stefan-Boltzmann's law using LST, emissivity, and T_a (Prata, 1996; Verma et al., 2016).

ECOSTRESS additionally computes ET using two other models, which are not provided as standard ET data products but are used to produce a multimodel uncertainty product as the standard deviation among the three models: a Penman-Monteith (Monteith, 1965)-based model (PM-Mu) (Mu et al., 2007, 2011) and the Surface Energy Balance System (SEBS) (Su, 2002).

PM-Mu partitions total ET into ET_c, ET_s, and ET_i:

$$ET_c = \frac{\left(\Delta R_n f_c + \rho C_p D_a f_c g_B\right)\left(1 - f_{wet}\right)}{\Delta + \gamma\left(1 + \frac{g_B}{g_S}\right)} \tag{9}$$

$$ET_s = \frac{\left(\Delta R_{ns} + \rho C_p D_a f_c g_{as}\right) f_{wet}}{\Delta + \gamma \frac{g_{as}}{g_{tot}}} + \frac{\left(\Delta R_{ns} + \rho C_p D_a f_c g_{as}\right)\left(1 - f_{wet}\right)}{\Delta + \gamma \frac{g_{as}}{g_{tot}}} \tag{10}$$

$$ET_i = \frac{\left(\Delta R_{nc} F_c + \rho C_p D_a f_c g_{hrc}\right) f_{wet}}{\left(\Delta + \gamma \frac{g_{hrc}}{g_{vc}}\right)} \tag{11}$$

where C_p is the specific heat of air at constant pressure ($J \cdot kg^{-1} \cdot K^{-1}$), ρ is air density (kg/m^3), g_B is aerodynamic conductance of dry canopy (s/m), g_S is stomatal conductance, g_{vc} is aerodynamic canopy conductance, g_{hrc} is wet canopy conductance, g_{as} is soil aerodynamic conductance, and g_{tot} is soil total conductance. Mu et al. (2011) provide constants for the conductances in a biome-specific lookup table.

SEBS is a single-source approach that targets the sensible heat flux (H), calculating ET from the residual of the energy balance:

$$ET = \Lambda_r ET_{wet} \tag{12}$$

$$\Lambda_r = 1 - \frac{H - H_{wet}}{H_{dry} - H_{wet}} \tag{13}$$

$$H_{dry} = (R_n - G) \tag{14}$$

$$H_{wet} = (R_n - G - ET_{wet}) \tag{15}$$

where Λ_r is the relative evaporation, ET_{wet} is the wet limit of ET, H_{wet} is the wet limit of sensible heat flux, H_{dry} is the dry limit of sensible heat flux and H is the actual sensible heat flux (W/m^2). This was later updated to the TSEB model.

The ECOSTRESS L2 product is used for LST and broadband emissivity. Landsat is used for ancillary surface properties NDVI, SAVI, and albedo. MODIS is used for ancillary atmospheric properties (with cloud gap-filling from the National Centers for Atmospheric Prediction) and to gap-fill cloudy Landsat surface properties (MODIS surface products are provided as gap-filled multiday aggregates) (Famiglietti et al., 2018; Fisher & ECOSTRESS algorithm development team, 2015; Verma et al., 2016). PT-JPL, PM-Mu, and SEBS/TSEB are all forced with the same input data for shared variables, including uniform calculation of, for example, R_n and G. The multimodel uncertainty product provides spatiotemporally varying information, necessary because a constant uncertainty value cannot be applied to the ET estimates. This is due to non-Gaussian and spatiotemporally variable controls on ET, derived from Monte Carlo sensitivity experiments, Gaussian error propagation, and Method of Moments uncertainty quantification

Figure 2. The 155 eddy covariance sites from around the world, covering 14 vegetation classes (International Geosphere-Biosphere Programme; IGBP) and 15 climate zones (Köppen-Geiger), provided evapotranspiration validation data for ECOSTRESS across a wide range of conditions. Insets show landscape detail at a selection of sites.

(Fisher et al., 2005, 2008). More information and detail on all the approaches can be found in the respective references.

2.2. Eddy Covariance Data

Eddy covariance measurements of *LE* were collected for this study from 155 towers around the world from July 2018 (just after ECOSTRESS launch) to July 2019 (Figure 2 and supporting information Table S1). There were two ECOSTRESS recording gaps during this period (29 September to 5 December 2018 and 14 March to 15 May 2019) due to engineering anomalies that have since been resolved, thus limiting the full potential extent of coverage in the first year. Of those 155 sites, ECOSTRESS obtained clear-sky data during this period for 120 of the sites. The eddy covariance data also were not consistently continuous across all sites. After quality control on both ECOSTRESS and eddy covariance data, 82 sites were ultimately used. The majority of sites were located in North America (104), with additional sites spread across Europe (23), Central and South America (5), Africa (2), Asia (3), the Middle East (2), and Australia and New Zealand (16). Fifteen of the 23 Köppen-Geiger climate zones (Peel et al., 2007) were represented: humid subtropical, Cfa (27); temperate oceanic, Cfb (24); warm-summer humid continental, Dfb (24); hot-summer Mediterranean, Csa (17); cold semiarid, Bsk (16); tropical savanna, Aw (7); warm-summer Mediterranean, Csb (4); hot-summer humid continental, Dfa (8); warm, dry-summer continental, Dsb (4); hot semiarid, Bsh (5); subarctic, Dfc (3); monsoon-influenced hot-summer humid continental, Dwa (3); tropical monsoon, Am (2); hot deserts, Bwh (3); and cold desert, Bwk (1). Fourteen of the 17 International Geosphere-Biosphere Programme (IGBP) vegetation classes (Loveland et al., 1999) were represented, with the plurality in croplands (40); and the rest in evergreen needleleaf forests (26); grasslands (23); deciduous broadleaf forests, (22); open shrublands (9); savannas (6); evergreen broadleaf forests, EBF (6); permanent wetlands (5); woody savannas (5); closed shrublands (5); mixed forests (5); water bodies (1); cropland/natural vegetation mosaics (1); and deciduous needleleaf forests (1). Moreover, within vegetation classes there was large site variation, adding to the sampling diversity. Many different agricultural crops were included, ranging from corn and potatoes to almond orchards and rice fields, for example. Forest sites ranged from recently planted pine trees to 100 +year-old oak forests. Alpine grasslands, peat bogs, saltwater marshes, and desert grasslands also contributed to the diverse data set.

Large synthesis databases coinciding with the recent time period of this analysis were not yet available, so we collated sites individually. Potential sites were identified from a wide variety of methods and sources:

AmeriFlux (ameriflux.lbl.gov), FLUXNET (fluxnet.fluxdata.org/sites/site-list-and-pages), EuroFlux (europe-fluxdata.eu), OzFlux (ozflux.org.au), AsiaFlux (asiaflux.net), NEON (neonscience.org), Tropi-Dry/Enviro-net (tropi-dry.org; enviro-net.org), literature review, and personal communication. Additionally, site point of contacts (POCs) or principal investigators (PIs) were asked if they knew of other sites in the region. We developed individualized emails based on research of the contacts and sites, and networks or other connections, to establish a social connection to facilitate response. Data from 35% of the sites (54) came from flux data networks; data from the other 101 sites were received directly from PIs. Coauthorship (and gratitude) was offered for data use. Introduction to other site POCs/PIs by already established partners led to a higher likelihood of positive response and subsequent data contribution and collaboration. Nearly every contact made led to at least an attempt to contribute data. The flux community in general was very supportive and interested in supporting a new and novel NASA mission linked directly to their shared science interests.

Each site POC/PI was contacted to discuss a number of details, including the operational status of their tower from July 2018 onward, verification of site descriptive information, confirmation of the required variables, and ability to deliver data relatively quickly (e.g., <1 month). To facilitate participation, a suggested formatting, delivery, and quality assurance/quality control (QAQC) was offered, but not required. As such, multiple data delivery mechanisms, formats, and QAQC were ultimately ingested. Data came from email attachments, institutional servers and websites, automatic SFTP and FTP downloads, and continuously updated internet-based services such as Google sheets. More than a dozen data formats were received across DAT, ASCII, text, Microsoft Excel (XLSX), comma/tab separated value (CSV/TSV), Hierarchical Data Format (HDF/H5), WINACE (.C**, .m**, .s**), Touchstone/SnP (s34, s46, c00, m34, and m36), and Block Compression (BC1).

The data received varied widely in level of processing, from extensive to raw. As needed, we formatted data for consistency, including renaming data gaps with NaN, conversion of timestamps to ECOSTRESS timestamps, and resampling of time steps finer than 30 min to 30-min time steps (for ease of analysis, understanding that ECOSTRESS does not overpass exactly on the hour/half-hour). We matched data to quality flags and excluded data that were flagged from the source data as either "poor quality" or "not a direct observation" (Foken et al., 2004; Foken & Wichura, 1996; Göckede et al., 2008). Given the recency of these data, we identify these data as initial estimates, which may be subject to change once ingested into repositories and network-wide QA/QC applied. This limits the quality of our analysis, partially obviated by the large number of sites.

Finally, we processed the data through the FLUXNET 2015 data processing standards and code for half-hourly energy balance closure (fluxnet.fluxdata.org/data/fluxnet2015-dataset/data-processing) (Foken, 2008; Stoy et al., 2013; Twine et al., 2000; Wilson et al., 2002). The method produces a range of uncertainty on the eddy covariance measurements as well. The method requires data availability for LE, R_n, H, and G; 30% of the 155 sites were unable to provide all of these data, in which cases the statistical distribution in energy balance closure across all available sites was applied to these sites. The range in lack of closure across the sites varied from 10% (Q1, 25th %), 30% (Q2, median), and 50% (Q3, 75th %). As such, we included these closure quartiles to those 30% of sites that did not provide enough data for site-specific closure, flagging them, and those sites with Q3 energy balance closure, for additional assessment. These sites were given energy balance closures of 30% with uncertainties ranging from 10% to 50%. Ultimately, we found that these flagged sites mostly did not noticeably degrade the comparison against ECOSTRESS.

2.3. Analysis

ECOSTRESS instantaneous LE (time of overpass), uncertainty, quality flags, and cloud mask were used in this analysis. For each daytime ECOSTRESS scene collected over a flux tower, a selection of 5 by 5 pixels (70 m × 70 m for each pixel) was extracted centered on the tower coordinates, providing a subset 350-m × 350-m scene for each site. The mean, median, and interquartile ranges were calculated for the 5 × 5 subset, as well as for a further refined subset of 3 × 3 pixels (210 m × 210 m) meant to mitigate impacts from landscape heterogeneity or smaller tower footprints. These subsets were selected based on conservative assumptions of general footprint sizes. Generally, the 5 × 5 and 3 × 3 statistics were not statistically significantly different from one another because eddy flux sites are commonly located in relatively homogeneous landscapes. Nonetheless, some sites (especially agricultural sites) were located in very heterogeneous areas, and differences in these calculations became more prevalent. We mostly used the 5 × 5 subset (70%) but

visually examined each site in Google Earth to determine when the 3 × 3 subset should be used instead (30%). Ideally, the spatially and temporally varying coordinates of each tower footprint ("footprint-aware") would be provided and ingested. This was not available, however; as such, the overall assessment of ECOSTRESS error also includes some (unquantified) error due to footprint uncertainty (Chasmer et al., 2011; DuBois et al., 2018; Montaldo & Oren, 2016; Xu et al., 2017). Dynamic footprint information should be included in future validations. For comparison, we also evaluated a 1-km box around each tower (not all sites were available for this larger comparison).

We used the ECOSTRESS L2 and L3 quality flags to filter for high quality ECOSTRESS data. The L3 quality flag product, which itself is the combination of the quality flags of all of the ancillary inputs such as MODIS and Landsat, is provided as integers but must be read as 8-, 16-, or 32-bit binaries. For example, with the MODIS Cloud Mask flag, one-bit representation number can reveal: the cloud mask status flag (Bit 0), the cloud mask cloudiness flag (Bits 1 and 2), day/night flag (Bit 3), sunglint flag (Bit 4), snow/ice flag (Bit 5), and surface type flag (Bits 6 and 7). To decode each flag, one needs to shift the bit to the proper location and read the appropriate length. Reading a quality flag 51 as an 8-bit binary would result in 00110011. In this example, Bit 0 (read from the right to left) = 1 and would mean the data are useful. Specifically, data marked with bad quality flags in the MODIS forcing data for clouds (MOD06; bit code 119 marks clear-sky conditions) and aerosol optical depth (MOD04; bit codes 85 or 119 mark good conditions) were avoided as they would introduce contamination into the ECOSTRESS ET retrieval. Users will also want to use the ECOSTRESS uncertainty product for assessment of the ET quality, especially relative to the magnitude of the retrieved ET estimate. After quality control and given available cloud-free and high-quality ECOSTRESS acquisitions during this time period, 82 sites and 502 acquisitions were ultimately used for analysis, representing the majority of available site-to-satellite data pairs (supporting information Figure S1).

Our analysis of ECOSTRESS to eddy covariance measurements includes basic metrics of correlation, absolute root-mean-square error (RMSE), and overall bias. We summarize these statistics across all sites, by IGBP vegetation class, Köppen-Geiger climate zone, and time of day. For visualization and reduction, we grouped the Köppen-Geiger climate zones into 7, the IGBP vegetation classes into 5, and the times of day into 3. The Köppen-Geiger climate zones included (I) Bsh and Bwh (n = 5); (II) Bsk (n = 15); (III) Bwk (n = 1); (IV) Aw and Cfa (n = 15); (V) Cfb (n = 13); (VI) Csa and Csb (n = 11); and (VII) Dfa, Dfb, Dwa, and Dsb (n = 22). The IGBP vegetation classes included (I) croplands (n = 23); (II) deciduous broadleaf forests and mixed forest (n = 13); (III) EBF (n = 2); (IV) evergreen needleleaf forests and deciduous needleleaf forests (n = 8); and (V) grasslands, savannas, woody savannas, permanent wetlands, and open shrublands (n = 36). The times of day included (I) <10 a.m. (n = 172); (II) 10 a.m. to 2 p.m. (n = 158); and (III) >2 p.m. (n = 172). We note that although there was large diversity in the sites, they do not necessarily sample a complete and unbiased statistical representation of the entire global land surface or their respective vegetation classes and climate zones (e.g., temperate sites are overrepresented); the available time window also precludes analyses of interannual variability and seasonal analyses. Future validations with a longer ECOSTRESS record and larger FLUXNET synthesis data sets should encompass such an analysis of representative distributions (e.g., Chu et al., 2017; Famiglietti et al., 2018).

3. Results

ET from ECOSTRESS (L3_ET_PT-JPL) compared well against a wide range of eddy covariance sites, vegetation classes, climate zones, and times of day (Figures 3–5). For instantaneous ET, the r^2 was 0.88, normalized (by range) RMSE was 6%, and overall bias was 8% (Figure 4). The overall RMSE was 41.3 W/m^2 compared to a mean of 182.0 W/m^2 and a range of 713.8 W/m^2. The mean absolute bias was 19%. The eddy covariance measurements were generally contained within ECOSTRESS uncertainty, which was often relatively well constrained (Figures 3 and 4).

Correlation, RMSE, and bias were generally uniformly good across all group differentiations (Figure 5). RMSE was relatively consistent across climate zones, though significantly lower in the Bwk and Csa-Csb climate zones. Bias was largest in the Bsh climate zone and consistently low across all the other climate zones. RMSE was also relatively consistent across vegetation classes, though significantly lower in the EBF class, and bias was largest in EBF. RMSE and bias were consistent across times of day. R^2 was generally consistent across climate zones, vegetation classes, and times of day.

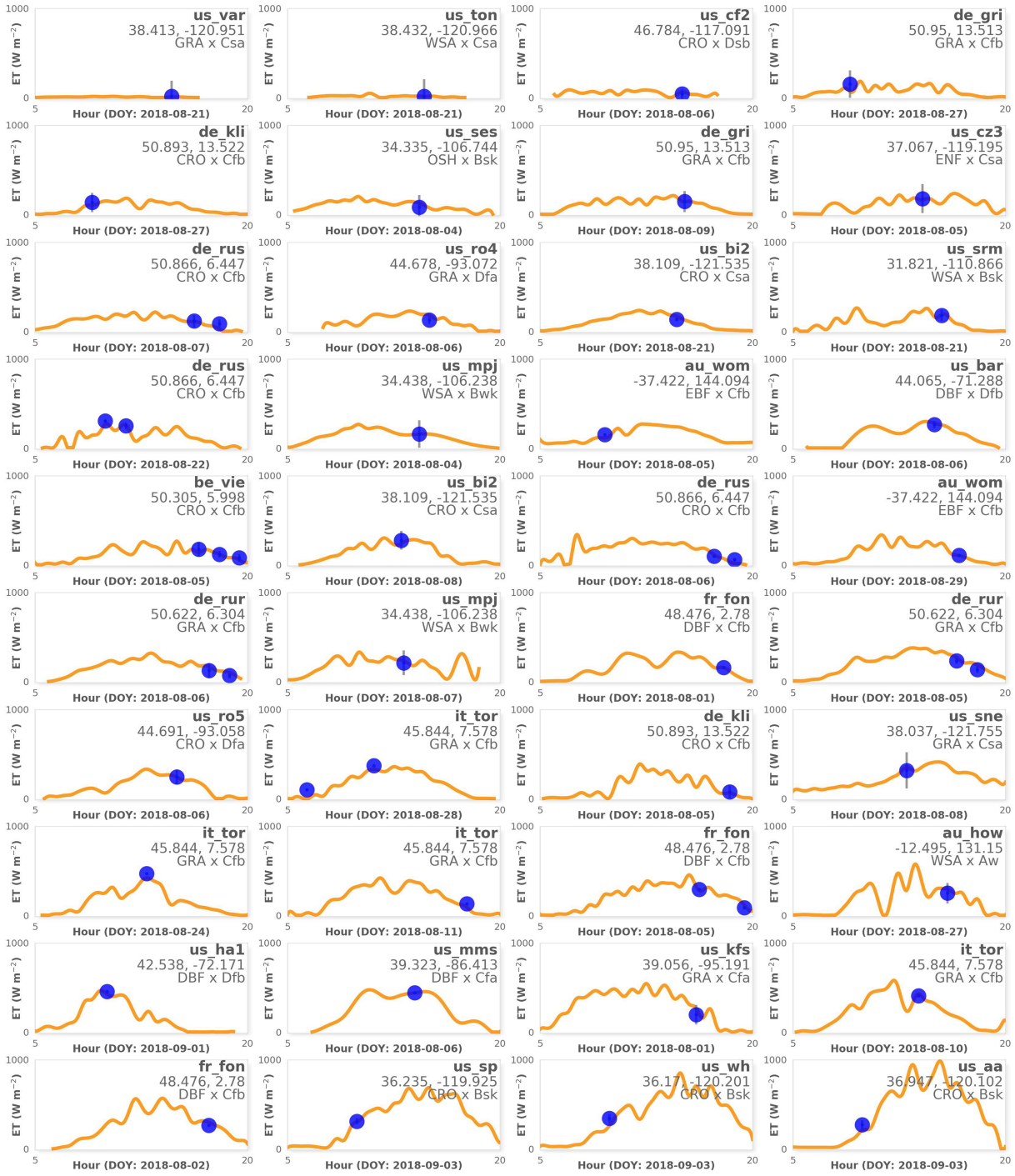

Figure 3. ECOSTRESS evapotranspiration (L3_ET_PT-JPL; blue with gray uncertainty bars) matches to a wide range of eddy covariance sites (orange) from around the world, covering 14 vegetation classes (International Geosphere-Biosphere Programme; IGBP) and 15 climate zones (Köppen-Geiger), sampling throughout the diurnal cycle. A selection of 40 sites is shown here for a single day for illustration, from dry (top) to wet (bottom). On occasion, multiple ECOSTRESS observations are taken throughout the same day at different times for a given site. Site name, latitude/longitude, vegetation class, and climate zone are given for each site in the top right of the subpanels.

For comparison, we evaluated a 1-km box around a subset of towers to provide insight into accuracy improvement with the ECOSTRESS high spatial resolution (Figure 6). As expected, most sites showed only marginal improvement with the high spatial resolution. This is because most FLUXNET sites are, by design, established in areas of relatively homogeneous surrounding land cover. However, many sites showed

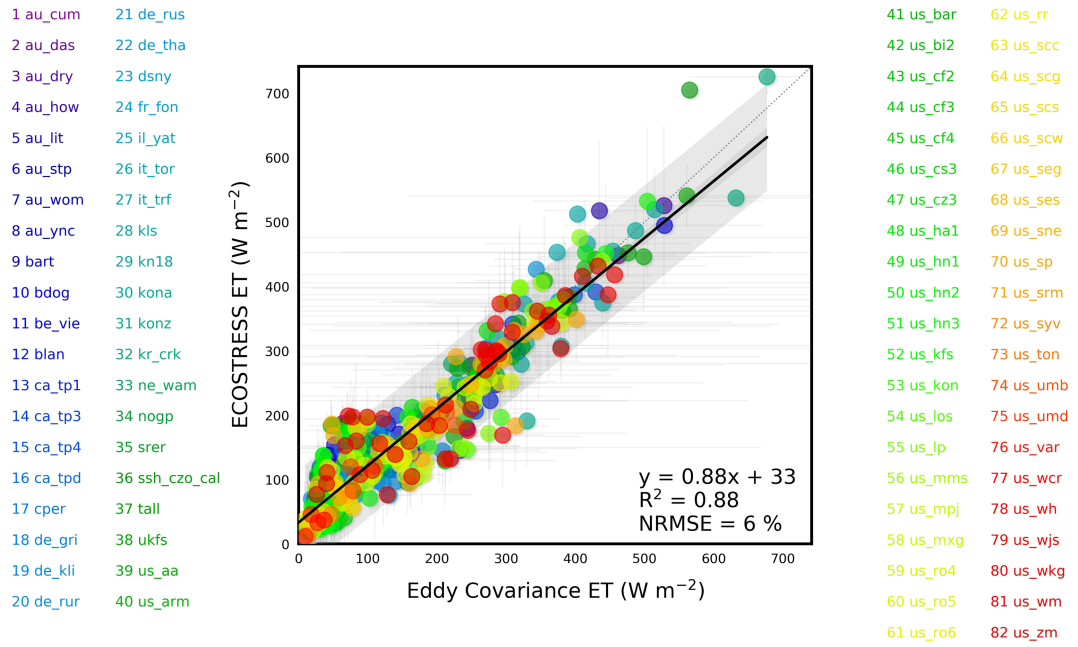

Figure 4. ECOSTRESS evapotranspiration (L3_ET_PT-JPL) aligns with in situ measurements of evapotranspiration from 82 eddy covariance sites (n = 502 points) from around the world. Data shown here are for the clear-sky instantaneous time of overpass. Each dot color corresponds to the text color of the site listed to the side of the scatterplot. Multimodel uncertainty (thin vertical gray lines) is assigned to the ECOSTRESS value, and energy balance closure uncertainty is assigned to the eddy covariance value (thin horizontal gray lines). The light gray shaded region around the regression is the 95% confidence interval, and the dark gray shaded region is the prediction interval.

marked improvement with the high spatial resolution. These sites were primarily agricultural, though some natural ecosystems also benefited from the high spatial resolution, due to large landscape heterogeneity around the respective sites. Generally, 1-km pixels underestimated eddy covariance ET. This means that the land surrounding flux sites tended to be drier than the flux site. This difference may be due to irrigation for agricultural sites, or generally good growing conditions for natural ecosystems (Jung et al., 2011). Relative to the eddy flux data, the high spatial resolution of ECOSTRESS ET improved correlation by 85% (0.76 to 0.89) and normalized RMSE by 62% (13% to 8%). Note that the error from a 1-km pixel from, for example, MODIS, may be even greater than we report because each of our 1-km boxes are centered perfectly on the tower site; a 1-km resolution imager would not necessarily be perfectly centered on each site.

4. Discussion

These results were for the initial, or Stage 1, validation. Although previous analyses have shown good performance of PT-JPL, results tend to be worse at the instantaneous level (generally better at daily/weekly/monthly aggregates) (Y. Chen et al., 2014; Ershadi et al., 2014; Fisher et al., 2008; Fisher et al., 2009; Jiménez et al., 2018; McCabe et al., 2016; Michel et al., 2016; Miralles et al., 2016; Polhamus et al., 2013; Purdy et al., 2018; Talsma et al., 2018; Vinukollu et al., 2011). Some studies have shown PT-JPL to have a high bias; so the small bias shown here was an improvement (Y. Chen et al., 2014; Jiménez et al., 2018; McCabe et al., 2016; Polhamus et al., 2013; Purdy et al., 2018; Talsma et al., 2018). We postulate that the results shown here are attributed to five main reasons: (I) the high spatiotemporal resolution of ECOSTRESS; (II) systematic eddy covariance energy balance closure computation; (III) overrepresentation of temperate ecosystems/underrepresentation of tropical ecosystems in the validation data set; (IV) careful treatment and filtering of the ECOSTRESS quality flags and cloud mask; and (V); the high accuracy and precision of the ECOSTRESS measurement, L2(LSTE) product, and the PT-JPL model itself.

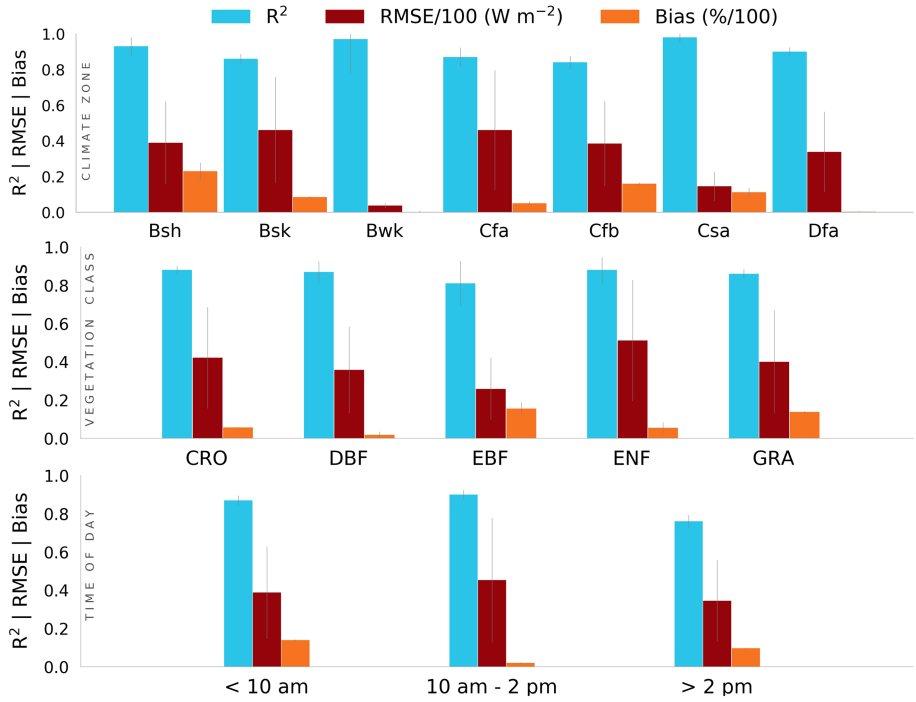

Figure 5. Coefficient of determination (blue), absolute RMSE (red), and overall bias (orange) are relatively consistent across climate zones (top), vegetation classes (middle), and times of day (bottom). The climate zones (Köppen-Geiger) included: (I) hot semiarid and hot desert (Bsh-Bwh); (II) cold semiarid (Bsk); (III) cold desert (Bwk); (IV) tropical wet and humid subtropical (Aw-Cfa); (V) temperate oceanic (Cfb); (VI) hot-summer Mediterranean and warm-summer Mediterranean (Csa-Csb); and (VII) hot-summer humid continental, warm summer humid continental, monsoon-influenced hot-summer humid continental, and Mediterranean-influenced hot-summer humid continental (Dfa-Dfb-Dwa-Dsb). The vegetation classes (International Geosphere-Biosphere Programme; IGBP) included (I) croplands (CRO); (II) deciduous broadleaf forests and mixed forests (DBF-MF); (III) evergreen broadleaf forests (EBF); IV) evergreen needleleaf forests and deciduous needleleaf forests (ENF-DNF); and (V) a combination of grasslands, savannas, woody savannas, wetlands, and open shrublands (GRA-SAV-WSA-WET-OSH).

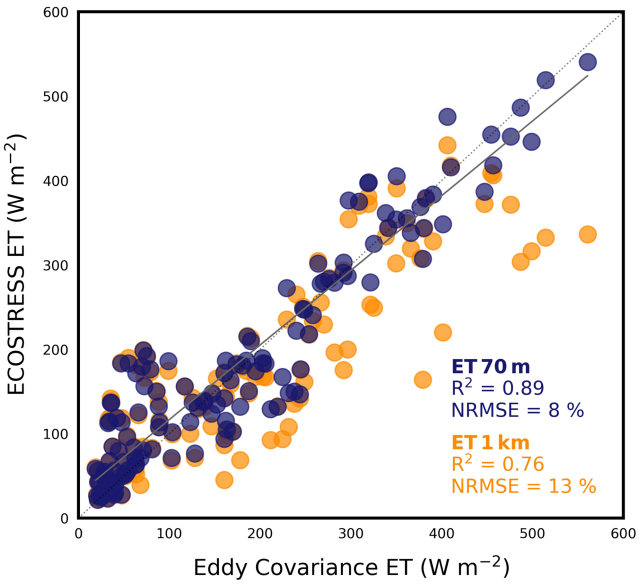

Figure 6. The accuracy of remotely sensed against eddy covariance evapotranspiration significantly improves with the high spatial resolution of ECOSTRESS (70 m, blue) relative to 1-km pixels (orange).

Previous global-scale analyses of remotely sensed ET products and algorithms, such as PT-JPL, have often been hindered by spatial resolutions at 1 km or greater (e.g., MODIS) (e.g., Jiménez et al., 2018; Purdy et al., 2018; Vinukollu et al., 2011; Yao et al., 2013). These resolutions introduce pixel-to-footprint mismatch comparing a single pixel to eddy covariance sites, which measure fluxes from footprints generally up to 1 km but usually much smaller, depending on tower height and wind conditions (Allen et al., 2005; Baldocchi, 1997; B. Chen et al., 2009; Göckede et al., 2004). Consequently, correlation coefficients may be decreased due to pixel contamination outside the footprint (e.g., from other land covers/uses) (e.g., Figure 6). In the case of ECOSTRESS, with 70-m pixels, multiple pixels are encompassed well within the approximately conservative footprint area here of 350 m × 350 m, or 210 m × 210 m, depending on the landscape conditions surrounding each site. This sampling provides good representation of the footprint while minimizing contamination. Still, as noted in the Methods, this comparison could be improved further by more detailed spatiotemporal information on footprint coordinates at each site (Montaldo & Oren, 2016; Xu et al., 2017). In comparison, Landsat-based ET validations contain comparable excellent spatial resolutions; but they often lack the frequency of ET retrievals and multisite validation due to limited temporal resolution (at most every 16 days) and challenges in

data production (ET is not produced operationally from Landsat as it is for ECOSTRESS) (e.g., Allen et al., 2005; Anderson et al., 2012; Senay et al., 2016).

Eddy covariance energy-balance closure varies significantly from site to site and even within a site from hour to hour and season to season (Da Rocha et al., 2009; Franssen et al., 2010; Leuning et al., 2012; Stoy et al., 2013; Wilson et al., 2002). What has not been historically well standardized, however, is how to correct the data to account for the error indicative by that lack of energy-balance closure (Baldocchi et al., 2001; Barr et al., 2006; Foken, 2008; Foken et al., 2011; Twine et al., 2000). The FLUXNET synthesis team, with contributions from the larger eddy flux community, has established rigorous postprocessing procedures for eddy covariance measurements, enabling a robust envelope of closure for all sites; this procedure was instituted in the FLUXNET 2015 synthesis data set (Moffat et al., 2007; Papale et al., 2012, 2006; Pastorello et al., 2017). Subsequently, a higher-quality eddy covariance observation is matched to the satellite-based estimate of ET. The goodness of fit metrics between site and satellite, therefore, are likely improved because of improvements in energy balance closure estimation and site level data quality.

It may be that the validation performance here is partially due to an overrepresentation of temperate ecosystems in the validation data set, and an underrepresentation of other ecosystems, especially in the tropics. ET in temperate ecosystems is typically easier to capture via satellite estimation than from tropical or semiarid ecosystems (Ershadi et al., 2014; Fisher et al., 2009, 2017, 2008; Jiménez et al., 2018; Jung et al., 2010; McCabe et al., 2016; Michel et al., 2016). Humid tropical ecosystems mix a multitude of species responses and water use rates with a high radiation and moisture environment, in addition to cloud interference to the remote measurement (Fisher et al., 2009; Gomis-Cebolla et al., 2019; Hasler & Avissar, 2007; Larson et al., 1999; Vergopolan & Fisher, 2016; Werth & Avissar, 2004). A small percentage error in tropical ET estimation can result in a large absolute flux error. ET from semiarid ecosystems is also challenging to estimate due to strong biotic, or atmospherically decoupled, control over ET, as opposed to abiotic, or atmospherically coupled, control largely dominating other ecosystems (Fisher et al., 2008; Fisher et al., 2017; García et al., 2013; Jarvis & McNaughton, 1986; Jung et al., 2010; Moyano et al., 2018; Nemani et al., 2003; Purdy et al., 2018). In contrast, ET in temperate ecosystems tends to be strongly coupled to atmospheric conditions, which also vary strongly diurnally and seasonally (Ershadi et al., 2014; Fisher et al., 2008; Jiménez et al., 2018; Jung et al., 2010; McCabe et al., 2016; Michel et al., 2016; Nemani et al., 2003; Purdy et al., 2018). As such, it is relatively easy to capture temperate ET so long as the atmospheric conditions are well tracked. Here, the majority of sites obtained were from the United States and temperate ecosystems, and under clear-sky conditions, which also improve retrieval accuracy. We chose to include all of the sites in the analysis as we did not have enough data to exclude or downweight/upweight sites for a more globally representative assessment, as we have done with much larger synthesis data sets (e.g., Famiglietti et al., 2018). But this may inflate the interpretation of ECOSTRESS performance at the global scale.

We cannot overstate the importance of incorporating the ECOSTRESS quality flags, cloud mask, and uncertainty product in analyses such as validations. Often, validations ignore the quality flags altogether—both from the satellite as well as in situ data, leading to incorrect assessment or attribution for error calculations. In the case of ECOSTRESS, the L3_ET_PT-JPL product is the result of a combination of multiple sources of data, each with their own quality flags and sources of error. These span from the ECOSTRESS L2 LSTE and cloud mask products derived from the calibrated L1 products and ancillary numerical weather prediction data, to the Landsat surface and MODIS atmospheric data, which include varying degrees of product levels. The quality flags of the Landsat and MODIS data are worth noting here. Given the coarse temporal resolution of Landsat, especially when cloudy, ECOSTRESS shifts reliance to MODIS for surface properties (NDVI, albedo) when the latest Landsat clear overpass becomes out of date (>16 days). This is now being improved with incorporation of Sentinel 2AB data. For the MODIS atmospheric properties, which are retrieved generally with some diurnal time separation to ECOSTRESS, if there happens to be a cloud beneath MODIS but not ECOSTRESS that day, then MODIS is in filled with numerical weather prediction data (e.g., backup algorithm). As such, ECOSTRESS is sharper when tied more closely to Landsat than to MODIS for the surface properties and more closely to MODIS than to the numerical weather prediction for the atmospheric properties. This may or may not have bearing on the comparison to the eddy flux site, depending on landscape homogeneity/heterogeneity surrounding the site. It may be possible to incorporate higher temporal resolution visible and near-infrared (VNIR) data from commercial cubesats (e.g., Planet) or other satellites in the future to enable more coincident overpasses with the TIR acquisition (Aragon et al., 2018). These

issues are relevant to future missions considering coincident versus separated TIR and VNIR measurements; ET uncertainty can be significant when the TIR-VNIR temporal separation is large, and phenological change (including agricultural harvest, deforestation, and leaf flush) is also significant (National Academies of Sciences, Engineering, and Medicine, 2018). Here, we took the quality flags and cloud mask into careful consideration at each site in order to ensure that the comparison against the eddy covariance measurement was directly tied to the ECOSTRESS retrieval for each site and day. The ECOSTRESS multimodel uncertainty product is the strongest predictor of ET quality. The larger uncertainty relative to the magnitude of the retrieved ET estimate, the more likely the estimate has lower accuracy.

Finally, the performance of the ECOSTRESS ET validation may be due in part to the high accuracy (<1 K) and precision (<0.2 K) of the ECOSTRESS measurement, the L2(LSTE) product, and the PT-JPL model itself (Hook et al., 2019). PT-JPL is controlled by multiple drivers, from surface temperature and vegetation characteristics to atmospheric properties, and the influence of those drivers varies depending on space and time (Badgley et al., 2015; Fisher et al., 2017, 2008; Polhamus et al., 2013; Ryu et al., 2011). While it is possible to generate an approximate estimate of ET from vegetation and atmospheric properties alone, LST dominates the ET signal at fine spatial scales, indicating when green vegetation is or is not transpiring (Fisher et al., 2017) (supporting information Figure S2). Because of this sensitivity to LST by PT-JPL, the accuracy and precision of the ECOSTRESS L2(LSTE) is critical to fine-scale ET estimates, such as in comparisons to eddy flux footprints (Fisher et al., 2013; García et al., 2013). In turn, the accuracy and precision of the L2(LSTE) product is a result of the ECOSTRESS instrument and L1 products themselves. ECOSTRESS was built with a state-of-the-art combination of thermal bands, blackbody calibrations, spatial resolution, temporal resolution, measurement accuracy, and precision, which, when used in conjunction with the established Temperature and Emissivity Separation and atmospheric correction retrieval algorithms, allows for a high-quality measurement that propagates upward through the higher-level ET and other data products.

5. Conclusion

ECOSTRESS provides new thermal infrared temperature measurements from the vantage point of the ISS at 70-m spatial resolution, every 1–5 days, and sampling the diurnal cycle. These measurements are used to generate a suite of data products, with the primary science focus on ET from the Level-3 latent heat flux (LE) product (L3_ET_PT-JPL). We produced a relatively rapid and robust preliminary first Stage 1 validation of ECOSTRESS clear-sky LE against 82 eddy covariance sites from around the world. ECOSTRESS LE matched well with site measurements (instantaneous: r^2 = 0.88; overall bias = 8%; normalized RMSE = 6%), showing good correlations and bias across a range of vegetation classes, climate zones, and times of day. This paper serves as a reference for the ECOSTRESS L3 ET accuracy and preliminary Stage 1 validation status for subsequent science that follows using these data.

Site-Level Acknowledgments

- Funding for AmeriFlux Management Project was provided by the U.S. Department of Energy's Office of Science under Contract N. DE-AC02-05CH11231.
- The funding by EU projects EUROFLUX, CARBOEUROFLUE, and CARBOEUROPE-IP, by German BMBF project ICOS-D and by the state of Saxony (TU Dresdon, LfULG) is greatly appreciated.
- USDA is an equal opportunity provider and employer. Funding for USDA authors comes from the ARS Office of National Programs (Projects 2036-61000-018-00-D, 8042-13610-029-00-D, 5012-21000-027-00D, and 2020-13660-008-00-D).
- Y. T. was supported in part by NASA NEWS program Grant NNX15AT41G. The CCZO project was sponsored by NSF CZO program Grant EAR-1331846.
- Research at the Yatir site is supported by the Israel Science Foundation, the Forestry Department, KKL, and the Wills and Lewis Center of the Weizmann Institute of Science, Israel.
- The US-KON and US-KFS Ameriflux sites are operated as a portion of the Konza Core Ameriflux site by NAB sponsored by the U.S. Department of Energy under a subcontract from DE-AC02-05CH11231.
- A. D. R. acknowledges support from the National Science Foundation (1637685). Research at the Bartlett Experimental Forest is supported by the USDA Forest Service's Northern Research Station.

- E. C. acknowledges data collection supported by AdaptMontBlanc project, cofunded by the European Regional Development Fund, under the operational program for territorial cooperation Italy-France (ALCOTRA).
- A. S.-A. acknowledges support from National Science and Engineering Research Council of Canada, Discovery Grant Program; Inter-American Institute for Global Change Research (CRN3-025); and Canadian Foundation for Innovation (CFI): Enviro-Net: Sensing of Changing Environment.
- M. F. M. and B. A. acknowledge support by the King Abdullah University of Science and Technology (KAUST).
- L. Š., N. K., and L. F. were supported by the Ministry of Education, Youth and Sports of CR within the CzeCOS program, Grant LM2015061, and within the National Sustainability Program I (NPU I), Grant LO1415.
- A. R. D. acknowledges support from the DOE Ameriflux Network Management Project award made to the ChEAS core site cluster, NSF CHEESEHEAD (AGS-1822420), the NSF North Temperate Lakes LTER (DEB-1440297), the Wisconsin Potato and Vegetable Growers Association, and the Wisconsin Department of Natural Resources.
- E. S. R. acknowledges support from the USDA-ARS supported Cook Agronomy Farm Long-Term Agro-ecosystem Research site.
- Data from the ne_waf and ne_wam stations (Niger) were collected in the framework of the AMMA-CATCH observatory (www.amma-catch.org), with funding from the French IRD, CNRS-INSU, and OREME institutes. Additional funding was granted by the ANR-Equipex CRITEX project (ANR-11-EQPX-0011). J.-P. Chazarin, A. Koné, A. Mamane, and M. Oï are thanked for their valuable technical contributions.
- M. A. A. acknowledges the Natural Sciences and Engineering Research Council (NSERC), Global Water Futures (GWF) Program, and the Ontario Ministry of Environment and Climate Change (MOECC), which supported CA-TP1, CA-TP3, CA-TP4 and CA-TPD sites.
- The US-Hn1, US-Hn2, and US-Hn3 sites are supported by the U.S. Department of Energy (DOE) Office of Biological and Environmental Research (BER) as part of BER's Subsurface Biogeochemical Research Program (SBR) at the Pacific Northwest National Laboratory (PNNL). PNNL is operated by Battelle Memorial Institute for the U.S. DOE under Contract DE-AC05-76RLO1830.
- M. L. G. acknowledges funding from the National Science Foundation through the Southern Sierra Critical Zone Observatory (EAR-1331939).
- The US-KON and US-KFS Ameriflux sites are operated as a portion of the Konza Core Ameriflux site by N. A. B. sponsored by the U.S. Department of Energy under a subcontract from DE-AC02-05CH11231.
- OzFlux data were provided through the Terrestrial Ecosystem Research Network (TERN), which is supported by the Australian government through the National Collaborative Research Infrastructure Strategy (NCRIS).
- KoFlux sites (CRK, GDK, GCK) were supported by National Research Foundation of Korea (NRF-2016M1A3A3A02018195 and NRF-2018R1C1B6002917) and Korea Forest Service (Korea Forestry Promotion Institute, Project 2017099A00-1719-BB01).
- M. S. acknowledges Terrestrial Environmental Observatories (http://www.tereno.net/overview-en?set_language=en).
- R. M. acknowledges support by the Natural Environment Research Council Award NE/R016429/1 as part of the UK-SCAPE program delivering National Capability.
- Texas Water Observatory is supported by Research Development Fund of Texas A&M University.
- C. E. M. and C. J. B. were partially funded by the DOE Center for Advanced Bioenergy and Bioproducts Innovation (U.S. Department of Energy, Office of Science, Office of Biological and Environmental Research under Award DE-SC0018420). Any opinions, findings, and conclusions or recommendations expressed in this publication are those of the author(s) and do not necessarily reflect the views of the U.S. Department of Energy.

Author Contributions

J. B. F. formulated the idea; J. B. F. designed the research; J. B. F., B. L., G. H. H., A. J. P., M. B. D., K. C.-N., and A. W. performed the research; R. G. A., B. A., M. A. A., D. D. B., J. M. B., H. B., C. J. B., C. B., S. C. B.,

G. B., N. B., B. C., S. C.-C., J. C., B. J. C., E. C., J. D., A. R. D., A.D. L., L. F., M. L. G., T. J. G., T. G., M. S. J., M. K., D. K., N. K., J.-H. L., I. M., M. F. M., J. E. C. M., B. P. M., C. M., L. M., R. M., J. W. M., G. P., A. D. R., E. S. R., Y. R., A. S.-A., E. S., I. S., L. S., and Y. T. provided the data; all authors contributed to the writing of the paper.

Conflict of Interest

The authors declare no conflict of interest.

Acknowledgments
We thank B. Freepartner, M. Sikka, F. Galvan, and R. Littles for software assistance. We thank Peter Blanken, James Cleverly, Higo Jose Dalmagro, Ken Davis, Eric Dufrene, Beverly Law, Marcy Litvak, Kim Novick, Matti Rasanen, Russell Scott, and Dan Yakir for contributing data. The journal editors and anonymous reviewers provided useful suggestions to improve the paper. The research was carried out at the Jet Propulsion Laboratory, California Institute of Technology, under a contract with the National Aeronautics and Space Administration. California Institute of Technology. Government sponsorship acknowledged. Support was provided by NASA's ECOSTRESS mission.

References

Allen, R. G., Pereira, L. S., Howell, T. A., & Jensen, M. E. (2011). Evapotranspiration information reporting: I. Factors governing measurement accuracy. *Agricultural Water Management*, *98*(6), 899–920.

Allen, R. G., Pereira, L. S., Raes, D., & Smith, M. (1998). *Crop evapotranspiration: Guidelines for computing crop water requirements (FAO Irrigation and Drainage Paper)* (p. 328). Rome: FAO - Food and Agriculture Organization of the United Nations.

Allen, R. G., Tasumi, M., Morse, A., & Trezza, R. (2005). A Landsat-based energy balance and evapotranspiration model in western US water rights regulation and planning. *Irrigation and Drainage Systems*, *19*(3–4), 251–268.

Allen, R. G., Tasumi, M., & Trezza, R. (2007). Satellite-based energy balance for mapping evapotranspiration with internalized calibration (METRIC)-model. *Journal of Irrigation and Drainage Engineering*, *133*, 380–394.

Anderson, M. C., Allen, R. G., Morse, A., & Kustas, W. P. (2012). Use of Landsat thermal imagery in monitoring evapotranspiration and managing water resources. *Remote Sensing of Environment*, *122*, 50–65.

Anderson, M. C., Hain, C., Otkin, J., Zhan, X., Mo, K., Svoboda, M., et al. (2013). An intercomparison of drought indicators based on thermal remote sensing and NLDAS-2 simulations with US Drought Monitor classifications. *Journal of Hydrometeorology*, *14*(4), 1035–1056.

Anderson, M. C., Hain, C., Wardlow, B., Pimstein, A., Mecikalski, J. R., & Kustas, W. P. (2010). Evaluation of drought indices based on thermal remote sensing of evapotranspiration over the continental United States. *Journal of Climate*, *24*(8), 2025–2044.

Anderson, M. C., Kustas, W. P., Hain, C. R., Cammalleri, C., Gao, F., Yilmaz, M., et al. (2013). Mapping surface fluxes and moisture conditions from field to global scales using ALEXI/DisALEXI, Remote sensing of energy fluxes and soil moisture content. 207–232.

Anderson, M. C., Kustas, W. P., Norman, J. M., Hain, C. R., Mecikalski, J. R., Schultz, L., et al. (2011). Mapping daily evapotranspiration at field to continental scales using geostationary and polar orbiting satellite imagery. *Hydrology and Earth System Sciences*, *15*, 223–239.

Aragon, B., Houborg, R., Tu, K., Fisher, J. B., & McCabe, M. (2018). CubeSats enable high spatiotemporal retrievals of crop-water use for precision agriculture. *Remote Sensing*, *10*(12), 1867.

Armanios, D. E., & Fisher, J. B. (2014). Measuring water availability with limited ground data: Assessing the feasibility of an entirely remote-sensing-based hydrologic budget of the Rufiji Basin, Tanzania, using TRMM, GRACE, MODIS, SRB, and AIRS. *Hydrological Processes*, *28*(3), 853–867.

Badgley, G., Fisher, J. B., Jiménez, C., Tu, K. P., & Vinukollu, R. K. (2015). On uncertainty in global evapotranspiration estimates from choice of input forcing datasets. *Journal of Hydrometeorology*, *16*(4), 1449–1455.

Baldocchi, D. (1997). Flux footprints within and over forest canopies. *Boundary-Layer Meteorology*, *85*(2), 273–292.

Baldocchi, D. (2008). 'Breathing' of the terrestrial biosphere: Lessons learned from a global network of carbon dioxide flux measurement systems. *Australian Journal of Botany*, *56*, 1–26.

Baldocchi, D., Falge, E., Gu, L. H., Olson, R. J., Hollinger, D., Running, S. W., et al. (2001). FLUXNET: A new tool to study the temporal and spatial variability of ecosystem-scale carbon dioxide, water vapor, and energy flux densities. *Bulletin of the American Meteorological Society*, *82*(11), 2415–2434.

Baldocchi, D. D. (2003). Assessing the eddy covariance technique for evaluating carbon dioxide exchange rates of ecosystems: Past, present and future. *Global Change Biology*, *9*(4), 479–492.

Barr, A., Morgenstern, K., Black, T., McCaughey, J., & Nesic, Z. (2006). Surface energy balance closure by the eddy-covariance method above three boreal forest stands and implications for the measurement of the CO_2 flux. *Agricultural and Forest Meteorology*, *140*(1–4), 322–337.

Bastiaanssen, W., Noordman, E., Pelgrum, H., Davids, G., Thoreson, B., & Allen, R. (2005). SEBAL model with remotely sensed data to improve water-resources management under actual field conditions. *Journal of Irrigation and Drainage Engineering*, *131*(1), 85–93.

Bouchet, R. J. (1963). Evapotranspiration re'elle evapotranspiration potentielle, signification climatique. *Rep. Publ. 62* (pp. 134-142. Berkeley, California: International Association for Hydrological Sciences.

Chasmer, L., Kljun, N., Hopkinson, C., Brown, S., Milne, T., Giroux, K., et al. (2011). Characterizing vegetation structural and topographic characteristics sampled by eddy covariance within two mature aspen stands using lidar and a flux footprint model: Scaling to MODIS. *Journal of Geophysical Research*, *116*, G02026. https://doi.org/10.1029/2010JG001567

Chen, B., Black, T. A., Coops, N. C., Hilker, T., Trofymow, J. T., & Morgenstern, K. (2009). Assessing tower flux footprint climatology and scaling between remotely sensed and eddy covariance measurements. *Boundary-Layer Meteorology*, *130*(2), 137–167.

Chen, X., Rubin, Y., Ma, S., & Baldocchi, D. (2008). Observations and stochastic modeling of soil moisture control on evapotranspiration in a Californian oak savanna. *Water Resources Research*, *44*, W08409. https://doi.org/10.1029/2007WR006646

Chen, Y., Xia, J., Liang, S., Feng, J., Fisher, J. B., Li, X., et al. (2014). Comparison of satellite-based evapotranspiration models over terrestrial ecosystems in China. *Remote Sensing of Environment*, *140*, 279–293.

Chu, H., Baldocchi, D. D., John, R., Wolf, S., & Reichstein, M. (2017). Fluxes all of the time? A primer on the temporal representativeness of FLUXNET. *Journal of Geophysical Research: Biogeosciences*, *122*, 289–307. https://doi.org/10.1002/2016JG003576

Da Rocha, H. R., Manzi, A. O., Cabral, O. M., Miller, S. D., Goulden, M. L., Saleska, S. R., et al. (2009). Patterns of water and heat flux across a biome gradient from tropical forest to savanna in Brazil. *Journal of Geophysical Research*, *114*, G00B12. https://doi.org/10.1029/2007JG000640

DuBois, S., Desai, A. R., Singh, A., Serbin, S. P., Goulden, M. L., Baldocchi, D. D., et al. (2018). Using imaging spectroscopy to detect variation in terrestrial ecosystem productivity across a water-stressed landscape. *Ecological Applications*, *28*(5), 1313–1324. https://doi.org/10.1002/eap.1733

Ershadi, A., McCabe, M. F., Evans, J. P., Chaney, N. W., & Wood, E. F. (2014). Multi-site evaluation of terrestrial evaporation models using FLUXNET data. *Agricultural and Forest Meteorology*, *187*, 46–61.
Falge, E., Baldocchi, D., Olson, R., Anthoni, P., Aubinet, M., Bernhofer, C., et al. (2001). Gap filling strategies for long term energy flux data sets. *Agricultural and Forest Meteorology*, *107*(1), 71–77.
Famiglietti, C. A., Fisher, J. B., Halverson, G., & Borbas, E. E. (2018). Global validation of MODIS near-surface air and dew point temperatures. *Geophysical Research Letters*, *45*, 7772–7780. https://doi.org/10.1029/2018GL077813
Farahani, H. J., Howell, T. A., Shuttleworth, W. J., & Bausch, W. C. (2007). Evapotranspiration: Progress in measurement and modeling in agriculture. *Transactions of the ASABE*, *50*(5), 1627–1638.
Fisher, J. B., Debiase, T. A., Qi, Y., Xu, M., & Goldstein, A. H. (2005). Evapotranspiration models compared on a Sierra Nevada forest ecosystem. *Environmental Modelling & Software*, *20*(6), 783–796.
Fisher, J. B., & ECOSTRESS algorithm development team (2015). ECOsystem Spaceborne Thermal Radiometer Experiment on Space Station (ECOSTRESS): Level-3 evapotranspiration LE (ET_PT-JPL) Algorithm Theoretical Basis Document (ATBD). *Rep*., 24 pp, Jet Propulsion Laboratory, Pasadena.
Fisher, J. B., & ECOSTRESS algorithm development team (2018). ECOsystem Spaceborne Thermal Radiometer Experiment on Space Station (ECOSTRESS): Level-4 Evaporative Stress Index L4(ESI_PT-JPL) Algorithm Theoretical Basis Document (ATBD) *Rep*., 8 pp, Jet Propulsion Laboratory, Pasadena.
Fisher, J. B., Malhi, Y., de Araújo, A. C., Bonal, D., Gamo, M., Goulden, M. L., et al. (2009). The land-atmosphere water flux in the tropics. *Global Change Biology*, *15*, 2694–2714.
Fisher, J. B., K. Mallick, J.-H. Lee, G. C. Hulley, C. G. Hughes, & S. J. Hook (2013). Uncertainty in evapotranspiration from uncertainty in land surface temperature, In *American Meteorological Society*. Austin, TX.
Fisher, J. B., Melton, F., Middleton, E., Hain, C., Anderson, M., Allen, R., et al. (2017). The future of evapotranspiration: Global requirements for ecosystem functioning, carbon and climate feedbacks, agricultural management, and water resources. *Water Resources Research*, *53*, 2618–2626. https://doi.org/10.1002/2016WR020175
Fisher, J. B., Tu, K., & Baldocchi, D. D. (2008). Global estimates of the land-atmosphere water flux based on monthly AVHRR and ISLSCP-II data, validated at 16 FLUXNET sites. *Remote Sensing of Environment*, *112*(3), 901–919.
Fisher, J. B., Whittaker, R. H., & Malhi, Y. (2011). ET Come Home: A critical evaluation of the use of evapotranspiration in geographical ecology. *Global Ecology and Biogeography*, *20*, 1–18.
Foken, T. (2008). The energy balance closure problem: An overview. *Ecological Applications*, *18*(6), 1351–1367. https://doi.org/10.1890/06-0922.1
Foken, T., Aubinet, M., Finnigan, J. J., Leclerc, M. Y., Mauder, M., & Paw, K. T. (2011). Results of a panel discussion about the energy balance closure correction for trace gases. *Bulletin of the American Meteorological Society*, *92*(4), ES13–ES18.
Foken, T., Göockede, M., Mauder, M., Mahrt, L., Amiro B., & Munger, W. (2004). Post-field data quality control, In *Handbook of Micrometeorology* (pp. 181–208). Springer.
Foken, T., & Wichura, B. (1996). Tools for quality assessment of surface-based flux measurements. *Agricultural and Forest Meteorology*, *78*(1–2), 83–105.
Franssen, H. H., Stöckli, R., Lehner, I., Rotenberg, E., & Seneviratne, S. I. (2010). Energy balance closure of eddy-covariance data: A multisite analysis for European FLUXNET stations. *Agricultural and Forest Meteorology*, *150*(12), 1553–1567.
García, M., Sandholt, I., Ceccato, P., Ridler, M., Mougin, E., Kergoat, L., et al. (2013). Actual evapotranspiration in drylands derived from in-situ and satellite data: Assessing biophysical constraints. *Remote Sensing of Environment*, *131*, 103–118.
Gaston, K. J. (2000). Global patterns in biodiversity. *Nature*, *405*(6783), 220–227.
Gillespie, A., Rokugawa, S., Matsunaga, T., Cothern, J. S., Hook, S., & Kahle, A. B. (1998). A temperature and emissivity separation algorithm for Advanced Spaceborne Thermal Emission and Reflection Radiometer (ASTER) images. *IEEE Transactions on Geoscience and Remote Sensing*, *36*(4), 1113–1126.
Göckede, M., Foken, T., Aubinet, M., Aurela, M., Banza, J., Bernhofer, C., et al. (2008). Quality control of CarboEurope flux data—Part 1: Coupling footprint analyses with flux data quality assessment to evaluate sites in forest ecosystems. *Biogeosciences*, *5*(2), 433–450.
Göckede, M., Rebmann, C., & Foken, T. (2004). A combination of quality assessment tools for eddy covariance measurements with footprint modelling for the characterisation of complex sites. *Agricultural and Forest Meteorology*, *127*(3–4), 175–188.
Gomis-Cebolla, J., Jimenez, J. C., Sobrino, J. A., Corbari, C., & Mancini, M. (2019). Intercomparison of remote-sensing based evapotranspiration algorithms over amazonian forests. *International Journal of Applied Earth Observation and Geoinformation*, *80*, 280–294.
Halverson, G. (2018). *Near real-time monitoring of global evapotranspiration and its application to water resource management*. Northridge, Northridge, California: California State University.
Hasler, N., & Avissar, R. (2007). What controls evapotranspiration in the Amazon Basin? *Journal of Hydrometeorology*, *8*, 380–395.
Hook, S. J., Cawse-Nicholson, K., Barsi, J., Radocinski, R., Hulley, G., Johnson, W., et al. (2019). In-flight validation of ECOSTRESS, Landsat 7 and 8 Thermal Infrared Spectral Channels using the Lake Tahoe CA/NV and Salton Sea CA Automated Validation Sites. *IEEE Transactions on Geoscience and Remote Sensing*, *58*(2), 1294–1302.
Hulley, G. C., & Hook, S. J. (2011). Generating consistent land surface temperature and emissivity products between ASTER and MODIS data for earth science research. *IEEE Transactions on Geoscience and Remote Sensing*, *49*(4), 1304–1315.
Hulley, G. C., & S. J. Hook (2018). ECOsystem Spaceborne Thermal Radiometer Experiment on Space Station (ECOSTRESS): Level-2 land surface temperature and emissivity Algorithm Theoretical Basis Document (ATBD). *Rep*., 96 pp, Jet Propulsion Laboratory, Pasadena.
Hulley, G. C., Malakar, N. K., Islam, T., & Freepartner, R. J. (2017). NASA's MODIS and VIIRS land surface temperature and emissivity products: A long-term and consistent earth system data record. *IEEE Journal of Selected Topics in Applied Earth Observations and Remote Sensing*, *11*(2), 522–535.
Iwabuchi, H. (2006). Efficient Monte Carlo methods for radiative transfer modeling. *Journal of the Atmospheric Sciences*, *63*(9), 2324–2339.
Jarvis, P. G., & McNaughton, K. G. (1986). Stomatal control of transpiration: Scaling up from leaf to region. *Advances in Ecological Research*, *15*, 1–49.
Jiménez, C., Martens, B., Gonzalez Miralles, D., Fisher, J. B., Beck, H. E., & Fernández-Prieto, D. (2018). Exploring the merging of the global land evaporation WACMOS-ET products based on local tower measurements. *Hydrology and Earth System Sciences*, *22*(8), 4513–4533.
June, T., Evans, J. R., & Farquhar, G. D. (2004). A simple new equation for the reversible temperature dependence of photosynthetic electron transport: A study on soybean leaf. *Functional Plant Biology*, *31*(3), 275–283.
Jung, M., Reichstein, M., Ciais, P., Seneviratne, S. I., Sheffield, J., Goulden, M. L., et al. (2010). Recent decline in the global land evapotranspiration trend due to limited moisture supply. *Nature*, *467*(7318), 951–954. https://doi.org/10.1038/nature09396

Jung, M., Reichstein, M., Margolis, H. A., Cescatti, A., Richardson, A. D., Arain, M. A., et al. (2011). Global patterns of land-atmosphere fluxes of carbon dioxide, latent heat, and sensible heat derived from eddy covariance, satellite, and meteorological observations. *Journal of Geophysical Research*, *116*, G00J07. https://doi.org/10.1029/2010JG001566

Kilic, A., Allen, R., Trezza, R., Ratcliffe, I., Kamble, B., Robison, C., & Ozturk, D. (2016). Sensitivity of evapotranspiration retrievals from the METRIC processing algorithm to improved radiometric resolution of Landsat 8 thermal data and to calibration bias in Landsat 7 and 8 surface temperature. *Remote Sensing of Environment*, *185*, 198–209.

Kobayashi, H., & Iwabuchi, H. (2008). A coupled 1-D atmosphere and 3-D canopy radiative transfer model for canopy reflectance, light environment, and photosynthesis simulation in a heterogeneous landscape. *Remote Sensing of Environment*, *112*(1), 173–185.

Larson, K., Hartmann, D. L., & Klein, S. A. (1999). The role of clouds, water vapor, circulation, and boundary layer structure in the sensitivity of the tropical climate. *Journal of Climate*, *12*, 2359–2374.

Leuning, R., Van Gorsel, E., Massman, W. J., & Isaac, P. R. (2012). Reflections on the surface energy imbalance problem. *Agricultural and Forest Meteorology*, *156*, 65–74.

Logan, T. L., & Johnson, W. R. (2015). ECOsystem Spaceborne thermal radiometer experiment on Space Station (ECOSTRESS): Level-1 focal plane Array and Radiometric Calibration Algorithm Theoretical Basis Document (ATBD). *Rep*., 18 pp, Jet Propulsion Laboratory, Pasadena.

Loveland, T. R., Zhu, Z., Ohlen, D. O., Brown, J. F., Reed, B. C., & Yang, L. (1999). An analysis of the IGBP global land-cover characterization process. *Photogrammetric Engineering and Remote Sensing*, *65*, 1021–1032.

Malakar, N. K., & Hulley, G. C. (2016). A water vapor scaling model for improved land surface temperature and emissivity separation of MODIS thermal infrared data. *Remote Sensing of Environment*, *182*, 252–264.

Marshall, M., Funk, C., & Michaelsen, J. (2012). Examining evapotranspiration trends in Africa. *Climate Dynamics*, *38*(9–10), 1849–1865.

Matricardi, M. (2008), The generation of RTTOV regression coefficients for IASI and AIRS using a new profile training set and a new line-by-line database, European Centre for Medium-Range Weather Forecasts.

McCabe, M. F., Ershadi, A., Jimenez, C., Miralles, D. G., Michel, D., & Wood, E. F. (2016). The GEWEX LandFlux project: Evaluation of model evaporation using tower-based and globally gridded forcing data. *Geoscientific Model Development*, *9*(1), 283–305.

Michel, D., Jiménez, C., Miralles, D., Jung, M., Hirschi, M., Ershadi, A., et al. (2016). TheWACMOS-ET project–Part 1: Tower-scale evaluation of four remote-sensing-based evapotranspiration algorithms. *Hydrology and Earth System Sciences*, *20*(2), 803–822.

Miralles, D., Jiménez, C., Jung, M., Michel, D., Ershadi, A., McCabe, M., et al. (2016). The WACMOS-ET project, part 2: Evaluation of global terrestrial evaporation data sets. *Hydrology and Earth System Sciences*, *20*(2), 823–842.

Miralles, D. G., Holmes, T. R. H., de Jeu, R. A. M., Gash, J. H., Meesters, A. G. C. A., & Dolman, A. J. (2011). Global land-surface evaporation estimated from satellite-based observations. *Hydrology and Earth System Sciences*, *15*(2), 453–469.

Miralles, D. G., Teuling, A. J., van Heerwaarden, C. C., & Vila-Guerau de Arellano, J. (2014). Mega-heatwave temperatures due to combined soil desiccation and atmospheric heat accumulation. *Nature Geoscience*, *7*(5), 345–349.

Moffat, A. M., Papale, D., Reichstein, M., Hollinger, D. Y., Richardson, A. D., Barr, A. G., et al. (2007). Comprehensive comparison of gap-filling techniques for eddy covariance net carbon fluxes. *Agricultural and Forest Meteorology*, *147*(3–4), 209–232.

Mölders, N., & Raabe, A. (1996). Numerical investigations on the influence of subgrid-scale surface heterogeneity on evapotranspiration and cloud processes. *Journal of Applied Meteorology*, *35*(6), 782–795.

Montaldo, N., & Oren, R. (2016). The way the wind blows matters to ecosystem water use efficiency. *Agricultural and Forest Meteorology*, *217*, 1–9.

Monteith, J. L. (1965). Evaporation and the environment. *Symposium of the Society of Exploratory Biology*, *19*, 205–234.

Moyano, M., Garcia, M., Palacios-Orueta, A., Tornos, L., Fisher, J., Fernández, N., et al. (2018). Vegetation water use based on a thermal and optical remote sensing model in the Mediterranean region of Doñana. *Remote Sensing*, *10*(7), 1105.

Mu, Q., Heinsch, F. A., Zhao, M., & Running, S. W. (2007). Development of a global evapotranspiration algorithm based on MODIS and global meteorology data. *Remote Sensing of Environment*, *111*, 519–536.

Mu, Q., Zhao, M., & Running, S. W. (2011). Improvements to a MODIS global terrestrial evapotranspiration algorithm. *Remote Sensing of Environment*, *111*, 519–536.

National Academies of Sciences, Engineering, and Medicine (2018). *Thriving on our changing planet: A decadal strategy for Earth observation from space* (p. 700). Washington, DC: The National Academies Press.

Nemani, R. R., Keeling, C. D., Hashimoto, H., Jolly, W. M., Piper, S. C., Tucker, C. J., et al. (2003). Climate-driven increases in global terrestrial net primary production from 1982 to 1999. *Science*, *300*(5625), 1560–1563. https://doi.org/10.1126/science.1082750

Oke, T. R. (1982). The energetic basis of the urban heat island. *Quarterly Journal of the Royal Meteorological Society*, *108*(455), 1–24.

Otkin, J. A., Anderson, M. C., Hain, C., Mladenova, I. E., Basara, J. B., & Svoboda, M. (2013). Examining rapid onset drought development using the thermal infrared–based Evaporative Stress Index. *Journal of Hydrometeorology*, *14*(4), 1057–1074.

Otkin, J. A., Anderson, M. C., Hain, C., & Svoboda, M. (2014). Examining the relationship between drought development and rapid changes in the evaporative stress index. *Journal of Hydrometeorology*, *15*(3), 938–956.

Papale, D., Agarwal, D. A., Baldocchi, D., Cook, R. B., Fisher, J. B., & van Ingen, C. (2012). Database maintenance, data sharing policy, collaboration. In M. Aubinet, T. Vesala, & D. Papale (Eds.), *Eddy covariance: A practical guide to measurement and data analysis* (pp. 399–424). New York: Springer.

Papale, D., Reichstein, M., Aubinet, M., Canfora, E., Bernhofer, C., Kutsch, W., et al. (2006). Towards a standardized processing of net ecosystem exchange measured with eddy covariance technique: Algorithms and uncertainty estimation. *Biogeosciences*, *3*(4), 571–583.

Pastorello, G., Papale, D., Chu, H., Trotta, C., Agarwal, D., Canfora, E., et al. (2017). A new data set to keep a sharper eye on land-air exchanges. *Eos Transactions American Geophysical Union (Online)*, *98*(8).

Peel, M. C., Finlayson, B. L., & McMahon, T. A. (2007). Updated world map of the Köppen-Geiger climate classification. *Hydrology and Earth System Sciences Discussions*, *4*(2), 439–473.

Polhamus, A., Fisher, J. B., & Tu, K. P. (2013). What controls the error structure in evapotranspiration models? *Agricultural and Forest Meteorology*, *169*, 12–24.

Potter, C. S., Randerson, J. T., Field, C. B., Matson, P. A., Vitousek, P. M., Mooney, H. A., & Klooster, S. A. (1993). Terrestrial ecosystem production: A process based model based on global satellite and surface data. *Global Biogeochemical Cycles*, *7*(4), 811–841.

Prata, A. J. (1996). A new long-wave formula for estimating downward clear-sky radiation at the surface. *Quarterly Journal of the Royal Meteorological Society*, *122*(533), 1127–1151.

Priestley, C. H. B., & Taylor, R. J. (1972). On the assessment of surface heat flux and evaporation using large scale parameters. *Monthly Weather Review*, *100*, 81–92.

Purdy, A., Fisher, J., Goulden, M., & Famiglietti, J. (2016). Ground heat flux: An analytical review of 6 models evaluated at 88 sites and globally. *Journal of Geophysical Research: Biogeosciences*, *121*, 3045–3059. https://doi.org/10.1002/2016JG003591

Purdy, A. J., Fisher, J. B., Goulden, M. L., Colliander, A., Halverson, G., Tu, K., & Famiglietti, J. S. (2018). SMAP soil moisture improves global evapotranspiration. *Remote Sensing of Environment*, *219*, 1–14.

Rabin, R. M., Stensrud, D. J., Stadler, S., Wetzel, P. J., & Gregory, M. (1990). Observed effects of landscape variability on convective clouds. *Bulletin of the American Meteorological Society*, *71*(3), 272–280.

Rind, D., Goldberg, R., Hansen, J., Rosenzweig, C., & Ruedy, R. (1990). Potential evapotranspiration and the likelihood of future drought. *Journal of Geophysical Research*, *95*(D7), 9983–10,004.

Ryu, Y., Baldocchi, D. D., Black, T. A., Detto, M., Law, B. E., Leuning, R., et al. (2012). On the temporal upscaling of evapotranspiration from instantaneous remote sensing measurements to 8-day mean daily-sums. *Agricultural and Forest Meteorology*, *152*(0), 212–222.

Ryu, Y., Baldocchi, D. D., Kobayashi, H., van Ingen, C., Li, J., Black, T. A., et al. (2011). Integration of MODIS land and atmosphere products with a coupled-process model to estimate gross primary productivity and evapotranspiration from 1 km to global scales. *Global Biogeochemical Cycles*, *25*, GB4017.

Ryu, Y., Jiang, C., Kobayashi, H., & Detto, M. (2018). MODIS-derived global land products of shortwave radiation and diffuse and total photosynthetically active radiation at 5 km resolution from 2000. *Remote Sensing of Environment*, *204*, 812–825.

Sahoo, A. K., Pan, M., Troy, T. J., Vinukollu, R. K., Sheffield, J., & Wood, E. F. (2011). Reconciling the global terrestrial water budget using satellite remote sensing. *Remote Sensing of Environment*, *115*(8), 1850–1865.

Saunders, R., Matricardi, M., & Brunel, P. (1999). An improved fast radiative transfer model for assimilation of satellite radiance observations. *Quarterly Journal of the Royal Meteorological Society*, *125*(556), 1407–1425.

Senay, G. B., Friedrichs, M., Singh, R. K., & Velpuri, N. M. (2016). Evaluating Landsat 8 evapotranspiration for water use mapping in the Colorado River Basin. *Remote Sensing of Environment*, *185*, 171–185.

Shukla, J., & Mintz, Y. (1982). Influence of land-surface evapotranspiration on the earth's climate. *Science*, *215*(4539), 1498–1501. https://doi.org/10.1126/science.215.4539.1498

Smyth, M., & Leprince, S. (2018). ECOsystem Spaceborne Thermal Radiometer Experiment on Space Station (ECOSTRESS): Level-1B resampling and Geolocation Algorithm Theoretical Basis Document (ATBD) *Rep*., 29 pp, Jet Propulsion Laboratory, Pasadena.

Stone, P. H., Chow, S., & Quirr, W. J. (1977). July climate and a comparison of January and July climates simulated by GISS general circulation model. *Monthly Weather Review*, *105*(2), 170–194.

Stoy, P. C., Mauder, M., Foken, T., Marcolla, B., Boegh, E., Ibrom, A., et al. (2013). A data-driven analysis of energy balance closure across FLUXNET research sites: The role of landscape scale heterogeneity. *Agricultural and Forest Meteorology*, *171*, 137–152.

Su, Z. (2002). The Surface Energy Balance System (SEBS) for estimation of turbulent heat fluxes. *Hydrology and Earth System Sciences*, *6*, 85–99.

Taha, H. (1997). Urban climates and heat islands: Albedo, evapotranspiration, and anthropogenic heat. *Energy and Buildings*, *25*(2), 99–103.

Talsma, C. J., Good, S. P., Jimenez, C., Martens, B., Fisher, J. B., Miralles, D. G., et al. (2018). Partitioning of evapotranspiration in remote sensing-based models. *Agricultural and Forest Meteorology*, *260*, 131–143.

Twine, T. E., Kustas, W. P., Norman, J. M., Cook, D. R., Houser, P. R., Meyers, T. P., et al. (2000). Correcting eddy-covariance flux underestimates over a grassland. *Agricultural and Forest Meteorology*, *103*(3), 279–300.

Vergopolan, N., & Fisher, J. B. (2016). The impact of deforestation on the hydrological cycle in Amazonia as observed from remote sensing. *International Journal of Remote Sensing*, *37*(22), 5412–5430.

Verma, M., Fisher, J. B., Mallick, K., Ryu, Y., Kobayashi, H., Guillaume, A., et al. (2016). Global surface net-radiation at 5 km from MODIS Terra. *Remote Sensing*, *8*(739), 1–20.

Vicente-Serrano, S. M., Beguería, S., & López-Moreno, J. I. (2010). A multiscalar drought index sensitive to global warming: The standardized precipitation evapotranspiration index. *Journal of Climate*, *23*(7), 1696–1718.

Vinukollu, R. K., Wood, E. F., Ferguson, C. R., & Fisher, J. B. (2011). Global estimates of evapotranspiration for climate studies using multi-sensor remote sensing data: Evaluation of three process-based approaches. *Remote Sensing of Environment*, *115*, 801–823.

Werth, D., & Avissar, R. (2004). The regional evapotranspiration of the Amazon. *Journal of Hydrometeorology*, *5*(1), 100–109.

Wilson, K., Goldstein, A., Falge, E., Aubinet, M., Baldocchi, D., Berbigier, P., et al. (2002). Energy balance closure at FLUXNET sites. *Agricultural and Forest Meteorology*, *113*(1–4), 223–243.

Xu, K., Metzger, S., & Desai, A. R. (2017). Upscaling tower-observed turbulent exchange at fine spatio-temporal resolution using environmental response functions. *Agricultural and Forest Meteorology*, *232*, 10–22.

Yao, Y., Liang, S., Cheng, J., Liu, S., Fisher, J. B., Zhang, X., et al. (2013). MODIS-driven estimation of terrestrial latent heat flux in China based on a modified Priestley–Taylor algorithm. *Agricultural and Forest Meteorology*, *171*, 187–202.

Zhang, Q., Xiao, X., Braswell, B. H., Linder, E., Aber, J., & Moore, B. (2005). Estimating seasonal dynamics of biophysical and biochemical parameters in a deciduous forest using MODIS data and a radiative transfer model. *Remote Sensing of Environment*, *99*, 357–371.

Zhao, M. S., Heinsch, F. A., Nemani, R. R., & Running, S. W. (2005). Improvements of the MODIS terrestrial gross and net primary production global data set. *Remote Sensing of Environment*, *98*, 164–176.

References From the Supporting Information

Acosta, M., Darenova, E., Dušek, J., & Pavelka, M. (2017). Soil carbon dioxide fluxes in a mixed floodplain forest in the Czech Republic. *European Journal of Soil Biology*, *82*, 35–42.

Arain, M. A., & Restrepo-Coupe, N. (2005). Net ecosystem production in a temperate pine plantation in southeastern Canada. *Agricultural and Forest Meteorology*, *128*(3), 223–241.

Beringer, J., Hutley, L. B., McHugh, I., Arndt, S. K., Campbell, D., Cleugh, H. A., et al. (2016). An introduction to the Australian and New Zealand flux tower network-OzFlux. *Biogeosciences*.

Brantley, S. L., White, T., West, N., Williams, J. Z., Forsythe, B., Shapich, D., et al. (2018). Susquehanna Shale Hills Critical Zone Observatory: Shale Hills in the context of Shaver's Creek watershed. *Vadose Zone Journal*, *17*(1).

Castro, S. M., Sanchez-Azofeifa, G. A., & Sato, H. (2018). Effect of drought on productivity in a Costa Rican tropical dry forest. *Environmental Research Letters*, *13*(4), 045001.

Chan, F. C., Arain, M. A., Khomik, M., Brodeur, J. J., Peichl, M., Restrepo-Coupe, N., et al. (2018). Carbon, water and energy exchange dynamics of a young pine plantation forest during the initial fourteen years of growth. *Forest Ecology and Management*, *410*, 12–26.
Cleverly, J., Boulain, N., Villalobos-Vega, R., Grant, N., Faux, R., Wood, C., et al. (2013). Dynamics of component carbon fluxes in a semi-arid Acacia woodland, central Australia. *Journal of Geophysical Research: Biogeosciences*, *118*, 1168–1185. https://doi.org/10.1002/jgrg.20101
Cook, B. D., Davis, K. J., Wang, W., Desai, A., Berger, B. W., Teclaw, R. M., et al. (2004). Carbon exchange and venting anomalies in an upland deciduous forest in northern Wisconsin, USA. *Agricultural and Forest Meteorology*, *126*(3–4), 271–295.
Desai, A. R., Bolstad, P. V., Cook, B. D., Davis, K. J., & Carey, E. V. (2005). Comparing net ecosystem exchange of carbon dioxide between an old-growth and mature forest in the upper Midwest, USA. *Agricultural and Forest Meteorology*, *128*(1), 33–55.
Desai, A. R., Xu, K., Tian, H., Weishampel, P., Thom, J., Baumann, D., et al. (2015). Landscape-level terrestrial methane flux observed from a very tall tower. *Agricultural and Forest Meteorology*, *201*, 61–75.
Galvagno, M., Wohlfahrt, G., Cremonese, E., Rossini, M., Colombo, R., Filippa, G., et al. (2013). Phenology and carbon dioxide source/sink strength of a subalpine grassland in response to an exceptionally short snow season. *Environmental Research Letters*, *8*(2), 025008.
Goulden, M., Anderson, R., Bales, R., Kelly, A., Meadows, M., & Winston, G. (2012). Evapotranspiration along an elevation gradient in California's Sierra Nevada. *Journal of Geophysical Research*, *117*, G03028. https://doi.org/10.1029/2012JG002027
Griebel, A., Bennett, L. T., Metzen, D., Cleverly, J., Burba, G., & Arndt, S. K. (2016). Effects of inhomogeneities within the flux footprint on the interpretation of seasonal, annual, and interannual ecosystem carbon exchange. *Agricultural and Forest Meteorology*, *221*, 50–60.
Hutley, L. B., Beringer, J., Isaac, P. R., Hacker, J. M., & Cernusak, L. A. (2011). A sub-continental scale living laboratory: Spatial patterns of savanna vegetation over a rainfall gradient in northern Australia. *Agricultural and Forest Meteorology*, *151*(11), 1417–1428.
Kang, M., Ruddell, B. L., Cho, C., Chun, J., & Kim, J. (2017). Identifying CO_2 advection on a hill slope using information flow. *Agricultural and Forest Meteorology*, *232*, 265–278.
Krupková, L., Havránková, K., Krejza, J., Sedlák, P., & Marek, M. V. (2019). Impact of water scarcity on spruce and beech forests. *Journal of Forestry Research*, *30*(3), 899–909.
Krupková, L., Marková, I., Havránková, K., Pokorný, R., Urban, O., Šigut, L., et al. (2017). Comparison of different approaches of radiation use efficiency of biomass formation estimation in mountain Norway spruce. *Trees*, *31*(1), 325–337.
Lathuillière, M. J., Dalmagro, H. J., Black, T. A., Arruda, P. H. Z. D., Hawthorne, I., Couto, E. G., & Johnson, M. S. (2018). Rain-fed and irrigated cropland-atmosphere water fluxes and their implications for agricultural production in southern Amazonia. *Agricultural and Forest Meteorology*, *256-257*, 407–419.
Lee, M. S., Hollinger, D. Y., Keenan, T. F., Ouimette, A. P., Ollinger, S. V., & Richardson, A. D. (2018). Model-based analysis of the impact of diffuse radiation on CO_2 exchange in a temperate deciduous forest. *Agricultural and Forest Meteorology*, *249*, 377–389.
Leuning, R., Cleugh, H. A., Zegelin, S. J., & Hughes, D. (2005). Carbon and water fluxes over a temperate Eucalyptus forest and a tropical wet/dry savanna in Australia: Measurements and comparison with MODIS remote sensing estimates. *Agricultural and Forest Meteorology*, *129*(3–4), 151–173.
Ma, S., Baldocchi, D., Wolf, S., & Verfaillie, J. (2016). Slow ecosystem responses conditionally regulate annual carbon balance over 15 years in Californian oak-grass savanna. *Agricultural and Forest Meteorology*, *228-229*, 252–264.
McGloin, R., Šigut, L., Havránková, K., Dušek, J., Pavelka, M., & Sedlák, P. (2018). Energy balance closure at a variety of ecosystems in Central Europe with contrasting topographies. *Agricultural and Forest Meteorology*, *248*, 418–431.
Missik, J. E. C., Liu, H., Gao, Z., Huang, M., Chen, X., Arntzen, E., et al. (2019). Groundwater-River water exchange enhances growing season evapotranspiration and carbon uptake in a semiarid riparian ecosystem. *Journal of Geophysical Research – Biogeosciences*, *124*, 99–114. https://doi.org/10.1029/2018JG004666
Morillas, L., Hund, S. V., & Johnson, M. S. (2019). Water use dynamics in double cropping of rainfed upland rice and irrigated melons produced under drought-prone tropical conditions. *Water Resources Research*, *55*, 4110–4127. https://doi.org/10.1029/2018WR023757
Moureaux, C. (2006). Annual net ecosystem carbon exchange by a sugar beet crop. *Agricultural and Forest Meteorology*, *139*(1–2), 25–39.
NEON (2019). No Title, Edited.
Ney, P., & Graf, A. (2018). High-resolution vertical profile measurements for carbon dioxide and water vapour concentrations within and above crop canopies. *Boundary-Layer Meteorology*, *166*(3), 449–473.
Peichl, M., Brodeur, J. J., Khomik, M., & Arain, M. A. (2010). Biometric and eddy-covariance based estimates of carbon fluxes in an age-sequence of temperate pine forests. *Agricultural and Forest Meteorology*, *150*(7–8), 952–965.
Posse, G., Lewczuk, N., Richter, K., & Cristiano, P. (2016). Carbon and water vapor balance in a subtropical pine plantation. *iForest-Biogeosciences and Forestry*, *9*(5), 736.
Prescher, A.-K., Grünwald, T. & Bernhofer, C. (2010a). Land use regulates carbon budgets in eastern Germany: From NEE to NB*P*, 1016–1025 pp.
Prescher, A.-K., Grünwald, T., & Bernhofer, C. (2010b). Land use regulates carbon budgets in eastern Germany: From NEE to NBP. *Agricultural and Forest Meteorology*, *150*(7–8), 1016–1025.
Reed, D. E., Dugan, H. A., Flannery, A. L., & Desai, A. R. (2018). Carbon sink and source dynamics of a eutrophic deep lake using multiple flux observations over multiple years. *Limnology and Oceanography Letters*, *3*(3), 285–292.
Renchon, A. A., Griebel, A., Metzen, D., Williams, C. A., Medlyn, B., Duursma, R. A., et al. (2018). Upside-down fluxes down under: CO_2 net sink in winter and net source in summer in a temperate evergreen broadleaf forest. *Biogeosciences*, *15*, 3703–3716.
Ruehr, N. K., Martin, J. G., & Law, B. E. (2012). Effects of water availability on carbon and water exchange in a young ponderosa pine forest: Above- and belowground responses. *Agricultural and Forest Meteorology*, *164*, 136–148.
Scott, R. L., Biederman, J. A., Hamerlynck, E. P., & Barron-Gafford, G. A. (2015). The carbon balance pivot point of southwestern U.S. semiarid ecosystems: Insights from the 21st century drought. *Journal of Geophysical Research: Biogeosciences*, *120*, 2612–2624.
Scott, R. L., Jenerette, G. D., Potts, D. L., & Huxman, T. E. (2009). Effects of seasonal drought on net carbon dioxide exchange from a woody-plant-encroached semiarid grassland. *Journal of Geophysical Research*, *114*, G04004. https://doi.org/10.1029/2008JG000900
Sulman, B. N., Desai, A. R., Cook, B. D., Saliendra, N., & Mackay, D. S. (2009). Contrasting carbon dioxide fluxes between a drying shrub wetland in northern Wisconsin, USA, and nearby forests. *Biogeosciences*, *6*(6), 1115–1126.
Tatarinov, F., Rotenberg, E., Maseyk, K., Ogée, J., Klein, T., & Yakir, D. (2016). Resilience to seasonal heat wave episodes in a Mediterranean pine forest. *New Phytologist*, *210*(2), 485–496. https://doi.org/10.1111/nph.13791
Torn, M. (2016). AmeriFlux US-ARM ARM Southern Great Plains site- Lamont, edited, United States.

Urbanski, S., Barford, C., Wofsy, S., Kucharik, C., Pyle, E., Budney, J., et al. (2007). Factors controlling CO_2 exchange on timescales from hourly to decadal at Harvard Forest. *Journal of Geophysical Research*, *112*, G02020. https://doi.org/10.1029/2006JG000293

Velluet, C., Demarty, J., Cappelaere, B., Braud, I., Issoufou, H.-A., Boulain, N., et al. (2014). Building a field-and model-based climatology of local water and energy cycles in the cultivated Sahel–annual budgets and seasonality. *Hydrology and Earth System Sciences*, *18*(12), 5001–5024.

Yang, K., Ryu, Y., Dechant, B., Berry, J. A., Hwang, Y., Jiang, C., et al. (2018). Sun-induced chlorophyll fluorescence is more strongly related to absorbed light than to photosynthesis at half-hourly resolution in a rice paddy. *Remote Sensing of Environment*, *216*, 658–673.